High-resolution chemostratigraphy reveals a large $\delta^{13}C$ gradient in the ~1.56 Ga redox-stratified ocean

Jin Luo[1,2], Simon W. Poulton[3,4], Bo Chen[1], Lanyun Miao[1], Kai Chen[5], Haijing Sun[1], Zhenfei Wang[6], Guoxiang Li[1], Maoyan Zhu[1,2*]

[1]State Key Laboratory of Palaeobiology and Petroleum Stratigraphy, Nanjing Institute of Geology and Palaeontology, Chinese Academy of Sciences, Nanjing 210008, China

[2]College of Earth and Planetary Sciences, University of Chinese Academy of Sciences, Beijing 100049, China

[3]School of Earth and Environment, University of Leeds, Leeds LS2 9JT, UK

[4]International Research Frontiers Initiative, Earth-Life Science Institute, Tokyo Institute of Technology, Tokyo 152-8550, Japan

[5]Institute of Geology and Paleontology, Linyi University, Linyi 276000, China

[6]International Center for Isotope Effects Research, Nanjing University, Nanjing, 210023, China

*Corresponding email: myzhu@nigpas.ac.cn

Abstract

Reports of decimeter-scale eukaryotic fossils and oxygenation events in the Gaoyuzhuang Formation (~1.56 Ga, North China Craton) have provided valuable insight into potential links between life and the environment during the early Mesoproterozoic. However, the detailed nature of this relationship remains unclear, partly due to limited basin-wide stratigraphic framework. Here, we present high-resolution carbon isotope composition of carbonate and organic matter ($\delta^{13}C_{carb}$ and $\delta^{13}C_{org}$) profiles from two fossil-hosting sections, representing shallow and deeper water settings, to calibrate the timing of marine oxygenation and eukaryotic evolution, and to reveal coeval carbon cycle dynamics. Our high-resolution data display a relative dynamic $\delta^{13}C_{carb}$ pattern with four perturbations in the Gaoyuzhuang members III-IV and build up a causal link between oxygenation and eukaryotic evolution during the second perturbation. The $\delta^{13}C_{carb}$ values exhibit a narrow range, but a distinct ~2.5‰ isotopic gradient exists between shallow and deeper water during the third perturbation. By contrast, $\delta^{13}C_{org}$ values reflect a more stable, but larger, isotopic gradient (~7‰), implying decoupling of the carbon isotopic system. We propose that the $\delta^{13}C_{org}$ compositions of shallow and deeper waters were controlled by specific microbial communities in a redox-stratified water column and a larger deep-ocean DOC reservoir, whereas $\delta^{13}C_{carb}$ sensitivity was buffered by a large DIC reservoir. Our modeling also highlights that the coeval oxygenation events were able to drive the observed short-term $\delta^{13}C_{carb}$ gradient during the third perturbation. Our findings reveal positive feedback between eukaryotic evolution and environmental changes, with implications for understanding Mesoproterozoic carbon cycle dynamics and paleo-redox conditions.

Key words: Mesoproterozoic, life-environment coevolution, carbon isotope, chemostratigraphy, North China craton

Highlights

- Two $\delta^{13}C_{carb}$ reference curves from fossil-hosting sections are established.
- A redox-stratified water column induced an ~7‰ $\delta^{13}C_{org}$ gradient in the ocean.
- The sensitivity of shallow water $\delta^{13}C_{carb}$ was likely buffered by a large DIC pool.
- Remineralization of the deep-water DOC pool induced an ~2.5‰ $\delta^{13}C_{DIC}$ gradient.
- O_2 concentrations at ~1.56 Ga drove the evolution of early large-scale eukaryotes.

1. Introduction

The composition of inorganic ($\delta^{13}C_{carb}$) and organic ($\delta^{13}C_{org}$) carbon isotopes in the ocean is influenced by a variety of environmental factors, such as weathering, atmospheric CO_2 concentration, the burial rates of carbonate minerals and organic carbon, and microbial processing (Hollander and McKenzie, 1991; Romanek et al., 1992; Bartley and Kah, 2004; Oehlert et al., 2012). These factors could influence the biological fixation of CO_2 by photosynthetic organisms, either directly by altering carbon availability or indirectly through changes in ocean chemistry and nutrient cycling. Therefore, reconstructing $\delta^{13}C$ compositions in the ancient ocean can provide crucial insight into carbon cycle dynamics and biogeochemical change over geological time (Kump and Arthur, 1999; Hotinski et al., 2004; Ahm and Husson, 2022). Between the two intervals of significant carbon isotope instability associated with planetary oxygenation in the Paleoproterozoic and Neoproterozoic (Hoffman et al., 1998; Bekker and Kaufman, 2007; Bekker et al., 2008; Johnston et al., 2012), the $\delta^{13}C_{carb}$ record during the mid-Proterozoic (~1.8-0.8 Ga) has until recently been considered to reflect a state of long-term stability, with values of ~-3‰ to +3‰ documenting relative environmental and biospheric stasis over this billion-year interval (e.g., Buick et al., 1995; Brasier and Lindsay, 1998; Bartley and Kah, 2004). However, detailed studies of carbon isotope systematics during the Mesoproterozoic are rare, which precludes a full understanding of the operation of the carbon cycle and potential links to environmental and biological evolution during this immense interval of time.

Recent reports of decimeter-sized multicellular eukaryotes from Member III of the Gaoyuzhuang Formation on the North China Craton (NCC), as well as geochemical analyses of oceanic redox changes, have unveiled a more dynamic environmental and biological perspective during the early Mesoproterozoic era (~1.56 Ga) than previously envisaged (e.g., Zhu et al., 2016; Zhang et al., 2018;

Shang et al., 2019; Luo et al., 2021; Xu et al., 2023). However, although geochemical studies have implicated enhanced environmental oxygenation as a driver for the evolution of the Gaoyuzhuang macrofossils, their ultimate relationship remains ambiguous. This is because detailed geochemical studies on precise fossil-bearing sections are largely absent, and a reliable stratigraphic correlation between different study areas across the Yanliao basin during the Gaoyuzhuang period has not been constructed. Furthermore, the operation of the oceanic carbon cycle at this time, which is closely linked to the evolution of the marine ecosystem and surface environments, remains poorly constrained (e.g., Guo et al., 2013; Luo et al., 2014).

To address these issues, we report two high-resolution carbon isotope profiles from members III and IV of the Gaoyuzhuang Formation, with a focus on both carbonate and organic carbon isotopes. Importantly, our sections represent two macrofossil-bearing localities (the Qianxi and Kuancheng sections), allowing us to calibrate the relationship between eukaryotic evolution and environmental oxygenation. In addition, the two sections document shallow and deeper water facies, providing an ideal platform to reconstruct the operation of the carbon cycle across this critical interval of biological evolution, from both a temporal and spatial perspective.

2. Geological background and depositional setting

2.1 Geological background

After a prolonged period of extensional tectonic activity that formed a NE-trending rift basin in the Yanliao area during the late Paleoproterozoic, the North China Craton became tectonically stable during the Meso-Neoproterozoic, with widespread deposition of carbonates in a stable epicontinental sea (Fig. 1A, B; Chu et al., 2007; Lu et al., 2008). The Gaoyuzhuang Formation is the first formation of

93 the Mesoproterozoic Jixian Group, which has a regionally disconformable contact with the underlying
94 Dahongyu Formation, reflecting tectonic uplift in the late Paleoproterozoic, and is conformably
95 overlain by the widespread marine red beds of the Yangzhuang Formation (Lu et al., 2008; Zhu et al.,
96 2022).

97 The carbonate-dominated Gaoyuzhuang Formation is commonly divided into four lithological
98 members based on sedimentology and inferred shallowing-upward sequences of stratotype section in
99 Jixian area (Fig. 1C). In general, Member I is characterized by the basal conglomerate or ripple-marked
100 shoreface sandstones that transition into cherty dolomicrite, with intercalated clay-rich and
101 stromatolitic dolomicrite in the middle to upper parts. Member II includes Mn-rich sediments,
102 dominantly consisting of thin, planar beds of Mn-rich dolomicrite and siltstones in the lower part,
103 followed by a transition to massive Mn-rich dolosparite in the upper part. The lower part of Member
104 III records a regional marine transgression from shallow subtidal to deeper shelf conditions,
105 approaching or even below storm wave base. The upper part of Member III, which is dominated by
106 massive bedded carbonates and columnar stromatolites, documents a marine regression and a return
107 to subtidal depositions. Member IV comprises thick, coarse-grained stromatolitic dolostone and an
108 overlying unit of dolomicrite with chert nodules. However, the sedimentary characteristics of different
109 Gaoyuzhuang localities have been influenced by rifting in the basin and the specific depositional setting
110 (Fig. 1D), which we describe in detail in the following section.

111 The geochronological framework for the Proterozoic sequence in the NCC has been well
112 established, although additional high-precision geochronology is required. For the Gaoyuzhuang
113 Formation, a tuff layer intercalated with sediments of the lower part of Member III in the Jixian region
114 yielded a zircon U-Pb (LA-ICP-MS) age of 1577 ± 12 Ma (Li et al., 2010). Additionally, zircon U-Pb ages

115 of 1560 ± 5 Ma (LA-ICP-MS) and 1559 ± 12 Ma (SHRIMP) have been reported from a tuff bed in the
116 upper part of Member III in Yanqing County (Li et al., 2010; Tian et al., 2015). A recently obtained tuff
117 U-Pb age of 1588.8 ± 6.5 Ma from the upper part of Gaoyuzhuang member III in the Qianxi section
118 specifically provides a constraint on the age of the Gaoyuzhuang macrofossils (Chen et al., 2024). These
119 ages suggest that deposition of Gaoyuzhuang Member III spanned ~15 million years.

120 A variety of eukaryotic fossils have been reported from the Gaoyuzhuang Formation, particularly
121 for Member III (Fig. 1C). For example, the most striking decimeter-sized carbonaceous macrofossils
122 occur in the lower part of Gaoyuzhuang Member III in the Qianxi section, displaying an unusual degree
123 of morphological complexity for the Mesoproterozoic eukaryotes (Zhu et al., 2016; Chen et al., 2023).
124 In addition, carbonaceous fragments of fossils, which preserve multicellular structures, have also been
125 found in the Kuancheng section (Zhu et al., 2016).

126 *2.2 Depositional setting of the study sections*

127 The sedimentary distribution of the Gaoyuzhuang Formation was controlled by the Yanliao fault-
128 depression basin, leading to a large variability in stratigraphic thickness of between ~80 to ~1990 m
129 (Zhu et al., 2022). Our researcb

130 The Qianxi and Jixian sections are considered to represent the accumulation center of the basin
131 during Gaoyuzhuang deposition, as they are characterized by the largest stratigraphic thickness of over
132 1500 m. The basal Gaoyuzhuang Formation in Qianxi is characterized by ~4 m of conglomerate, with
133 an unconformity above the ferruginous weathering crust of the upper Dahongyu Formation. Here,
134 Member III is dominated by dolostones, with a series of sedimentary cycles controlled by coeval sea
135 level change. The lower part of Member III in here characterized by a medium - thin bedded dolomite
136 with a few greenish siltstone interbeds. These carbonate deposits alternately show storm-agitated
137 deformation structures and parallel bedding (Fig. 2A), showing that the depositional setting
138 transitioned between middle and outer subtidal environments, close to or above the storm-wave base.
139 The decimeter-sized macrofossils were discovered in two layers of dolostone at a depth of ~225m in

the profile, roughly corresponding to the third sea level rise in the Gaoyuzhuang Formation (Fig. 2B). The macro-carbonaceous fossils are highly compressed and covered by a thin bed of calcareous mud, probably introduced by a large storm event (Zhu et al., 2016; Chen et al., 2023). The carbonates in Gaoyuzhuang Member IV are dominated by the massive-bedded cherty and stromatolitic dolomites with a well-developed teepee structure, indicating the depositional setting returned to shallow water with long-term evaporation (Fig. 2C and D). Similarly, Member III-IV of the Gaoyuzhuang Formation in Jixian section cover about 900 m, although some intervals are covered. The boundary of Member II and Member III in the Jixian section is marked by a transition from thick-bedded Mn-rich carbonate to medium-thickness limy dolostone. Above this, the lower part of Member III preserves a ~2m interval of nodule limestones, suggesting that the depositional setting was below the storm-wave base and deeper than that of the Qianxi section. A $\delta^{13}C_{carb}$ negative excursion, reaching to -3‰, has been reported above the nodule limestone horizon (Zhang et al., 2018). At the boundary of Gaoyuzhuang Member III and Member IV in the Jixian section, a set of molar-tooth structures and crystal fan are observed, indicating a unique seawater chemistry at the time in this area (Fang et al., 2022; Liu et al., 2023). Similar to the Qianxi section, the sedimentary facies of Member IV are featured by the thick stromatolitic dolostones with chert nodules, indicating a sea-level fall.

Compared to the Qianxi and Jixian section, the sedimentation rate in the Kuancheng area was much lower, with only ~400 m of sediments for Gaoyuzhuang members III-IV. The basal Gaoyuzhuang Formation conformably overlies thick-bedded sandstones of the upper Dahongyu Formation, suggesting water depths in this area were deeper, which is also supported by the lithologies present and higher organic matter contents (Fig. 3). The boundary between Member II and Member III is characterized by a transition from banded Mn-rich dolostone with ripple mark structures, to nodular limey dolostone intercalated with limey mudstones and shales, indicating deepening of the water depth, perhaps to below storm-wave base for the lower part of Member III. Fossil fragments with delicate multicellular structures have been found in thin-bedded dark grey muddy limestones from the lower part of Member III (Fig. 3B, ~0 m). Member IV in Kuancheng is composed of thick bedded to massive cherty dolosparite, representing a sea level regression to a shallower environment, similar to that seen in the Qianxi section.

In conclusion, Member III of the Gaoyuzhuang Formation in the Qianxi section deposited in a

relatively shallow shelf environment, mostly in a shallow-middle subtidal setting close to or above storm-wave base. For the Kuancheng section, where the lower part of Member III is charactered by organic-rich, thin-bedded carbonates and shales, deposition occurred in a deeper, low-energy environment, likely in a slope or basinal setting when the largest transgression occurred. Member IV in both sections documents a shallower depositional setting, characterized by massive cherty and stromatolitic dolostones.

3. Materials and methods

We collected 308 carbonate samples from Gaoyuzhuang members III and IV in the Qianxi section, covering approximately 1000 m of stratigraphy. Additionally, 30 samples were taken from the main macrofossil-hosting horizon in the same area, which is ~70 cm thick. A further 340 samples were collected from upper Member II to the lower part of Member IV in the Kuancheng section, covering approximately 400 m of stratigraphy. All samples were analyzed for $\delta^{13}C_{carb}$, while 149 samples from the Qianxi section and 106 samples from the Kuancheng section were additionally analyzed for total organic carbon (TOC) concentrations and $\delta^{13}C_{org}$. These data are supplemented by new TOC and $\delta^{13}C_{org}$ analyses of 92 carbonate samples with relatively high TOC contents from members III and IV of the Jixian section, where $\delta^{13}C_{carb}$ were previously reported by Luo et al. (2021).

All carbonate samples were cut to remove weathered surfaces and then powdered using an agate mortar prior to analysis of $\delta^{13}C_{carb}$, $\delta^{18}O$, $\delta^{13}C_{org}$ and TOC contents. For $\delta^{13}C_{carb}$ and $\delta^{18}O$ analyses, approximately 0.1 mg of whole rock powdered sample was reacted with 105% dry H_3PO_4 at 70°C on the Kiel IV carbonate device to ensure complete conversion of carbonate to CO_2. Carbon and oxygen isotopic compositions of the liberated CO_2 were then measured using the MAT 253 mass spectrometer. $\delta^{13}C_{carb}$ and $\delta^{18}O$ results were reported relative to the Vienna Pee Dee Belemnite (V-PDB) standard.

191 The working standard used during the analyses was GBW-04405 ($\delta^{13}C_{carb}$ = 0.57 ± 0.03‰, $\delta^{18}O$ = −8.49
192 ± 0.14‰), calibrated through NBS 19 and LSVEC. The external precisions (1σ) of working standards
193 during the measurements were <0.05‰ for $\delta^{13}C_{carb}$ and <0.1‰ for $\delta^{18}O$.

194 For $\delta^{13}C_{org}$ and TOC analyses, about 1 g of sample powder was fully decarbonated using 3 N HCl
195 for over 12 h. The residues were then repeatedly rinsed with deionized water until a neutral pH was
196 achieved, after which the carbonate-free residues were dried at 70°C for 48 h. First, about 20mg
197 decalcified samples were weighed for TOC analyses using an Elementor Macro Cube element analyzer.
198 The working standard Sulphanilamide (TOC = 41.81 wt. %) was used to monitor the analytical
199 uncertainties. The analytical precision for wt. % is ± 0.5%. Then about 0.5 - 40 mg of dried residues,
200 depending on measured TOC results, were placed in tin capsules and flash-combusted at 960 °C to
201 convert organic carbon to CO_2 using the Flash EA 2000, followed by isotopic compositions
202 measurements by the Delta V Advantage Isotope Ratio Mass Spectrometer. This process can generate
203 comparable CO_2 peak intensities between very low TOC samples and higher TOC samples, minimizing
204 uncertainty for the low TOC samples. Additionally, before each sample sequence, we conduct five
205 blank tests and five blank tin capsule tests to evaluate the impact of blank contamination. No
206 detectable CO_2 peaks were observed, indicating minimal interference from blanks or external
207 contamination. The δ value of organic carbon isotope was reported relative to the VPDB standard. For
208 every 12 samples, there are two working standards GBW-04407 ($\delta^{13}C_{org}$ = -22.43‰) and B215 ($\delta^{13}C_{org}$
209 = -28.85‰) ,and calibrated using USGAS40 and USGS42, with a measurement precision (1σ) of better
210 than 0.2‰.

4. Results

Paired carbon isotope and TOC analyses are shown in Figs. 4-5 and all data are presented in Supplementary Tables. Carbonate samples from the Qianxi section have low TOC contents (<0.1 wt. %), differing from samples from the Kuancheng section, which have TOC contents as high as 1.37 wt. % (0.69 ± 0.27 wt. %).

The $\delta^{13}C_{carb}$ profile in the Qianxi section has a relatively narrow range of between -1.63‰ to 0.60‰, while the Kuancheng section shows more variability in frequency, with values ranging between -2.33‰ and 0.08‰ (Fig. 4). Despite this, both sections have similar average $\delta^{13}C_{carb}$ values (-0.78 ± 0.46‰ in Qianxi; -0.74 ± 0.41‰ in Kuancheng), with distinct trends in the data that can be matched across both sections. Notably, in the Kuancheng section, a significant negative excursion is observed in the lower part of Member III (the third sedimentary cycle, ~52 to ~58 m), which may correspond to the minor negative excursion between 220 to 425 m in the Qianxi section. Additionally, there are then two distinct excursions to lighter $\delta^{13}C_{carb}$ values in both sections within Member III (from the base to ~78 m and ~80 to ~208 m in the Qianxi section, and at -82 to -52 m and -20 to 26 m in the Kuancheng section). Both sections then show a slight negative excursion in the lower part of Member IV (~500 to ~740 m in Qianxi, and ~86 to ~183 m at Kuancheng), which is followed by a positive shift to ~0.60‰ at Qianxi and 0.08‰ at Kuancheng in the upper part of Member IV. Intriguingly, these $\delta^{13}C_{carb}$ changes generally coincide with sedimentary cycles, despite the approximately four times lower sedimentation rate (based on the thickness of the sections) in the Kuancheng section, suggesting an environmental control on the $\delta^{13}C_{carb}$ dynamics.

While the ranges in $\delta^{13}C_{carb}$ are similar at both sites, the $\delta^{13}C_{org}$ compositions have a larger degree of variability between sections, with values of -28.33 ± 2.27‰ in Qianxi, and -31.76 ± 3.29‰ in

Kuancheng (Fig. 4). The $\delta^{13}C_{org}$ compositions are stable in both areas, although minor and localized fluctuations are observed. For example, lighter $\delta^{13}C_{org}$ values in the Qianxi area occur roughly coincident with transitions to deeper water depths, characterized by enhanced input of muddy sediments (at ~16 m, 88 m, 2`02m, 380 m, 451 m and 694 m). In addition, the low TOC samples from the lower part of Member III (at -72 to -53.1 m) in the Kuancheng section have distinct positive $\delta^{13}C_{org}$ values (> -30‰) relative to the other samples, although $\delta^{13}C_{carb}$ values are similar, while a small positive excursion (from -35.5‰ to -30.47‰) occurs from 59 to 87 m, coincident with a trend towards increased $\delta^{13}C_{carb}$ compositions.

The main horizon bearing in situ macrofossils in the Qianxi section occurs at ~225 m (Fig. 4, red arrow). At higher resolution, the $\delta^{13}C_{carb}$ profile for samples across this part of the section is generally controlled by lithological changes related to water depth variability (Fig. 5). In particular, there are two transitions to generally lighter $\delta^{13}C_{carb}$ and $\delta^{13}C_{org}$ values, corresponding to samples that have higher TOC contents (Fig. 5).

5. Discussion

5.1 Evaluation of $\delta^{13}C$ signatures

5.1.1 Diagenetic alteration

Diagenesis can potentially overprint the primary geochemical signatures of carbonate through interactions with diagenetic and post-diagenetic fluids, which commonly decrease carbonate oxygen isotope values (Banner and Hanson, 1990; Brand and Veizer, 1981; Swart and Oehlert, 2018). Therefore, to minimize potential effects of diagenetic alteration we exclude 23 samples (see supplementary table

S2) with $\delta^{18}O_{carb}$ values below -8‰ from the following discussion. For the remaining samples, we observe no significant correlation between either $\delta^{18}O_{carb}$ vs. $\delta^{13}C_{carb}$ or $\delta^{18}O_{carb}$ vs. $\delta^{13}C_{org}$ for both the Qianxi and Kuancheng sections (Fig. 6). Additionally, both sections display a similar $\delta^{18}O_{carb}$ pattern, characterized by an increasing trend from the base of the member III and peaking in the middle to upper part (Fig. 4). This trend supports the interpretation that the $\delta^{13}C_{carb}$ and $\delta^{18}O_{carb}$ compositions of these carbonate samples have not been significantly altered by meteoric waters or diagenetic fluids (Kaufman and Knoll, 1995). In addition, samples from the Kuancheng section have lower $\delta^{18}O_{carb}$ and $\delta^{13}C_{org}$ values relative to those in Qianxi section. Despite these differences, both sections display a similar range in $\delta^{13}C_{carb}$ values. The low grade of metamorphism (prehnite-pumpellyite facies) and relatively low degree of thermal alteration, further suggests that the $\delta^{13}C$ signatures in both carbonate and organic matter dominantly reflect primary conditions (Chu et al., 2007; Luo et al., 2014). Thus, post-depositional alteration is unlikely to have significantly impacted the secular patterns we observe, particularly since $\delta^{13}C$ compositions tend to record the compositions of precursor dolomites (Banner and Hanson, 1990).

5.1.2 Limited input of detrital organic matter

The influence of terrestrial organic matter on $\delta^{13}C_{org}$ values would be expected to be minor during the Mesoproterozoic, due to limited evidence for an extensive land biota (Selden and Edwards, 1989; Retallack et al., 2021). However, since our samples are from a continental margin basin, it is important to evaluate the potential impact of terrestrial organic matter input on the carbon isotope system, particularly in the case of the shallower water Qianxi section.

Carbonate samples from the Qianxi section show no correlation between Al contents and either $\delta^{13}C_{carb}$ or $\delta^{13}C_{org}$, in addition to essentially no correlation between Al and TOC or TOC and $\delta^{13}C_{org}$ (Fig. 7 A-D). In addition, there is no distinct difference in the behavior of carbon isotopes between samples with TOC below and above 0.05 wt. % (Fig. 4), suggesting no additional organic source for the more TOC-rich shallow water carbonates. As such, detrital input of organic matter appears to have played a negligible role in the $\delta^{13}C_{org}$ signatures in this area.

Our higher resolution investigation of the in-situ fossil-hosting horizon demonstrates a likely weathering influence on the carbon isotope system on a relatively short-term time scale (Fig. 7 E-H). Across this horizon, the samples show a weak negative correlation between Al and $\delta^{13}C_{carb}$ (Fig. 7E), potentially indicating that weathering may have enhanced the input of dissolved inorganic carbon (DIC), bringing lighter $\delta^{13}C$ signals to the nearshore environment. Furthermore, these samples also show a relatively strong positive correlation between TOC and Al contents when one sample with abnormally high TOC is removed (R^2=0.59, Fig. 7F). However, it remains important to identify whether higher TOC contents reflect an exogenous source (such as erosion of organic-rich shale), or whether this represents a preservation factor related to a higher input of clays or other siliciclastics. If the organic matter was additionally sourced from weathering of continental shale, no significant relationship should be apparent between Al and $\delta^{13}C_{org}$, or TOC and $\delta^{13}C_{org}$, due to the lack of isotope fractionation during weathering. However, the weak correlation between Al and $\delta^{13}C_{org}$ (Fig. 7G), and strong positive correlation between TOC and $\delta^{13}C_{org}$ (Fig. 7H), indicate that the $\delta^{13}C_{org}$ fractionations in these samples were likely controlled by primary productivity rather than detrital organic carbon. As such, an increased input of nutrients and oxidants during enhanced weathering likely induced higher rates of primary productivity, potentially even the development of temporary anoxia, and resulting in

296 lighter $\delta^{13}C_{org}$ values (Fig. 5). The higher clay mineral contents and sedimentation rates, in addition to
297 the enhanced potential for water column oxygen depletion, may also have aided the preservation of
298 the carbonaceous macrofossils.

299 Although samples from the deeper-water Kuancheng section have higher TOC contents than the
300 Qianxi section, these samples show essentially no correlation between Al and either $\delta^{13}C_{carb}$ or $\delta^{13}C_{org}$,
301 with weak correlations between Al vs. TOC and TOC vs. $\delta^{13}C_{org}$ (Fig. 7 I-L). This suggests no significant
302 influence from terrestrial organic matter, with $\delta^{13}C_{org}$ dominantly being controlled by productivity.
303 Although there is no significant difference in $\delta^{13}C_{carb}$ compositions between high and low TOC samples,
304 the different relationships between TOC and $\delta^{13}C_{org}$ for these two groups (Fig. 7L) potentially indicates
305 that the $\delta^{13}C_{org}$ fractionations were affected by different geochemical processes.

306

307 *5.2 $\delta^{13}C_{carb}$ Chemostratigraphy in the early Mesoproterozoic ocean*

308 The carbonate-carbon isotope record is widely used in stratigraphic correlation, particularly in the
309 Precambrian where biostratigraphy is not possible, as it may record synchronous carbon cycle
310 perturbations at the basinal or global scale (Knoll et al., 1986). In this study, we build upon our two
311 high-resolution carbon isotope profiles from the fossil-hosted sections of the Gaoyuzhuang Formation,
312 which currently provide the best $\delta^{13}C_{carb}$ reference curves for shallow and deeper-water facies during
313 the early Mesoproterozoic.

314 The $\delta^{13}C_{carb}$ values for members III and IV of the Gaoyuzhuang Formation are generally consistent
315 with typical $\delta^{13}C_{carb}$ records for the mid-Proterozoic, during which values tend to vary within a narrow
316 range of ~-3‰ to +3‰ (Brasier and Lindsay, 1998; Buick et al., 1995; Guo et al., 2013). However, our

detailed $\delta^{13}C_{carb}$ data reveal several perturbations that are coincident, at least across the Yanliao basin (Fig. 8). The integrated sedimentological and carbon isotope profiles for the four sections support four $\delta^{13}C_{carb}$ perturbations through members III (N1-N3) and IV (N4) of the Gaoyuzhuang Formation. These carbon isotope excursions can be distinguished in almost all the sections through different sedimentary facies, but to differing magnitudes, with the exception of the Jixian section which is affected by poor exposure and the low sampling resolution. Notably, In addition to correlative $\delta^{13}C_{carb}$ the sedimentary cycles are also comparable between the Qianxi and Kuancheng sections based on our detailed observations of sedimentary characteristics. The sedimentary cycle of the Gaoyuzhuang Member III was influenced by a significant transgression event, recognized as the largest transgression event during the Mesoproterozoic Jixian group in NCC. Our comprehensive field-based sedimentological analyses allow this transgression event to be further subdivided into three and a half sedimentary cycles, each of which comprises lithological change from thin bedded carbonate-dominated facies intercalated with shales, to carbonaceous shale-dominated facies, and then to thick-bedded and massive carbonate facies rich in chert nodules and bands as well as stromatolitic structures (Figs. 4, 8). This further supports the reliability of the stratigraphy correlation.

Despite variability in the sedimentary facies, depositional rates and $\delta^{13}C_{carb}$, the Qianxi section has a relatively narrow range in $\delta^{13}C_{carb}$ (0.6‰ to -1.6‰), and as such, the $\delta^{13}C_{carb}$ excursions are relatively minor in magnitude (Fig. 8). This pattern resembles that of the Jixian section, where most $\delta^{13}C_{carb}$ values are relatively stable at ~-0.5‰, but with a significant negative excursion reaching below -3‰ in the lower part of Member III. By contrast, in the deeper water settings represented by the Kuancheng and Yanqing sections, a higher degree of fluctuation in $\delta^{13}C_{carb}$ occurs, with negative excursions reaching values of ~-3.5‰.

At the boundary between Member II and Member III, the $\delta^{13}C_{carb}$ records for all sections transition from values of ~0‰ down to values of ~-1.0 to -1.5‰ (excursion N1), coincident with rising sea-level across the boundary. The N2 excursion is associated with the largest transgression in the lower part of Member III, where the depositional setting at Jixian, Kuancheng and Yanqing deepened to below storm-wave base. This excursion is accompanied by elevated I/(Ca+Mg) ratios and an increase in the isotopic composition of Mo in carbonates ($\delta^{98}Mo_{carb}$), likely indicating a widespread water column oxygenation event (Shang et al., 2019; Xu et al., 2023). The Gaoyuzhuang macrofossil assemblages are founded shortly after the N2 excursion (Zhu et al., 2016). The third $\delta^{13}C_{carb}$ anomaly (N3) represents the most negative value observed through the succession, with values reaching -3‰ in some areas (Fig. 8A). This excursion is followed by a positive shift that steadily returns to ~-0.5‰ in the upper part of Member III, coincident with a drop in sea level. Through the lower part of Member IV, $\delta^{13}C_{carb}$ values decrease to as low as -1.49‰ in the Qianxi section, -1.00‰ in the Jixian section, and -1.36‰ in the Kuancheng section (N4).

The higher resolution $\delta^{13}C_{carb}$ analyses for the fossil-hosting horizon at Qianxi clearly indicates a coincident small, but distinct, negative $\delta^{13}C_{carb}$ excursion (Fig. 5), which suggests a possible link between carbon cycle dynamics and early eukaryote evolution/preservation. In fact, the relationship between sedimentary cycles, coeval sea-level changes and periodic changes in $\delta^{13}C_{carb}$ and $\delta^{13}C_{org}$ observed in both the fossil-hosting horizon and the section as a whole suggests a potential control linked to orbital forcing. However, this suggestion requires further detailed study to evaluate.

359 *5.3 The carbon cycle in the early Mesoproterozoic ocean*

360 *5.3.1 Persistence of the $\delta^{13}C$ gradient across the basin*

361 Reconstructing the $\delta^{13}C$ gradient of the ancient ocean may provide crucial insight into marine
362 biogeochemical cycling over geological timescales, as it is predominantly driven by marine organisms
363 and their influence on the carbon cycle (Kump, 1991; Surge et al., 1997; Hotinski et al., 2004; Shen et
364 al., 2005; Li et al., 2018). In the modern ocean, the $\delta^{13}C$ gradient is maintained at ~-2‰ between the
365 surface and deep waters at a depth of ~1 km (oxygen minimum zone), which results from the combined
366 effect of the downward biological pump and the upward transport of carbon and nutrients through
367 upwelling (Kroopnick, 1974, 1985). Additionally, in anoxic settings like the Black Sea, the $\delta^{13}C_{carb}$
368 difference between surface and deep waters can reach ~-7‰, with an ~-4‰ difference in $\delta^{13}C_{org}$ from
369 shallow-to-deep sediments, which are attributed to limited vertical circulation within the basin and
370 the contribution of organic matter from different types of microbial metabolism (Deuser, 1970; Fry et
371 al., 1991; Karl and Knauer, 1991).

372 Our high-resolution $\delta^{13}C_{carb}$ chemostratigraphy of the Gaoyuzhuang Formation, combined with a
373 recently developed astronomical timescale, allows for the integration of four short-term $\delta^{13}C_{carb}$
374 perturbations from different environmental settings, with each $\delta^{13}C_{carb}$ perturbation spanning
375 approximately 1-2 million years (Fig. 9A, Liu et al., 2022). The narrow ranges in $\delta^{13}C_{carb}$ (<3‰) observed
376 in our samples align with previous $\delta^{13}C_{carb}$ records from Mesoproterozoic successions worldwide,
377 supporting the hypothesis of a large marine dissolved inorganic carbon reservoir in the Proterozoic
378 ocean, which buffered $\delta^{13}C_{carb}$ variability and the $\delta^{13}C_{DIC}$ gradient in shallow water carbonates
379 (Grotzinger and Kasting, 1993; Bartley and Kah, 2004; Hotinski et al., 2004; Bekker et al., 2008; Luo et
380 al., 2014). Furthermore, the synchronous changes in $\delta^{13}C_{carb}$ perturbations across the basin suggest a

381 good connection between the DIC reservoirs in shallow and deeper waters (Fig.8). However, lateral
382 $\delta^{13}C_{carb}$ variations are observed during the N3 interval, with values of -1.56‰ in the shallow carbonates
383 of the Qianxi section, ~-2.5‰ in mid-depth carbonates from the Jixian and Kuancheng sections, and -
384 3.5‰ in deeper water carbonates from the Kuancheng section. Such a gradient is significantly higher
385 than that reported for the Paleoproterozoic ocean at ~1.9 Ga (~0.5‰; Hotinski et al., 2004), but is
386 similar to a record for the early Cambrian ocean (~2.3‰; Li et al., 2018). While the effectiveness of the
387 biological pump would likely have been dampened by high pCO_2 and the large DIC flux during the early
388 Proterozoic (Hotinski et al., 2004), our $\delta^{13}C_{carb}$ data may reveal a potentially enhanced biological pump
389 effect during the N3 interval, along with a short-term reduction in the DIC reservoir, following a
390 transient oxygenation event and associated evolution the macroscopic photosynthetic organisms as
391 evidenced by the occurrence of the macroscopic fossils (Zhu et al., 2016).

392 Although the range in $\delta^{13}C_{carb}$ is relatively narrow, with a similar average value across our study
393 sections, the difference in $\delta^{13}C_{org}$ between the sections is noticeably larger and displays complex
394 isotopic behavior across different sedimentary facies (Fig. 9 B-E). Carbonate samples from the Qianxi
395 section, which were deposited in inter-subtidal environments, are characterized by heavier $\delta^{13}C_{org}$
396 values (ranging between ~-30‰ and ~-25‰) and very low TOC contents (<0.01 wt. %). The $\delta^{13}C_{org}$
397 values of most samples are relatively stable, with an average value of -27.97± 0.97‰, notwithstanding
398 a slight positive excursion during the N2 interval. On the other hand, the $\delta^{13}C_{org}$ compositions in the
399 Jixian, Kuancheng and Yanqing sections exhibit a negative excursion from ~-28‰ to ~-35‰ after the
400 N1 interval, followed by two slightly negative fluctuations during the N2 and N3 intervals. The largest
401 gradient in $\delta^{13}C_{org}$ of ~7‰ between the shallow and deeper environments is significantly greater than
402 the isotopic effect possible by heterotrophic reworking (Galimov, 2004).

403 Organic matter generated by photosynthetic organisms commonly induces smaller carbon
404 isotopic fractionation compared to anaerobic autotrophs (Hayes et al., 1999; Hollander and Smith,
405 2001). These isotopic offsets can be induced by the isotopic composition of the CO_2 the organisms
406 utilized, or changes in the partial pressure of CO_2 in the water column (Werne and Hollander, 2004).
407 Therefore, we propose a hypothesis to explain the observed ~7‰ $\delta^{13}C_{org}$ gradient based on differences
408 in microbial metabolism and carbon cycling within a redox-stratified ocean (Fig. 10). Samples from the
409 shallow-water Qianxi section were mainly deposited above the chemocline, where cyanobacteria
410 would have been the dominant primary producers. These primary producers preferentially utilized
411 light ^{12}C, thereby increasing the $^{13}C/^{12}C$ ratio in the carbon pool of the surface seawater and generating
412 free oxygen through oxygenic photosynthesis. The presence of sufficient oxidants in surface water
413 supported high organic carbon remineralization, preventing extensive organic carbon burial in the
414 shallow ocean, which is compatible with the very low TOC and relatively high $\delta^{13}C_{org}$ compositions
415 observed in Qianxi carbonates (Fig. 4). Furthermore, these oxygenated surface waters would have also
416 provided an ideal habitat to permit the evolution of the large Gaoyuzhuang eukaryotes (Zhu et al.,
417 2016).

418 By contrast, the samples from other study sections were mostly deposited below the chemocline
419 in anoxic settings. Anaerobic respiration of autotrophic organism would have been more intensive,
420 including methanotrophs that would generate very negative $\delta^{13}C_{org}$ values (Gong and Hollander, 1997;
421 Hinrichs et al., 2000; Yoshinaga et al., 2014). In addition, organic matter remineralization was also more
422 limited in the anoxic setting, leading to higher TOC in the sediments. Upwelling of carbon and nutrients
423 from deep waters may have been limited from a long-term perspective, further enlarging the $\delta^{13}C_{org}$
424 gradient between shallow and deeper waters and facilitating the deep-water DOC (dissolve organic

carbon) accumulation over time. Our hypothesis thus supports the existence of a larger DOC reservoir in the deep water than the shallow water, as proposed for the Paleoproterozoic and Neoproterozoic ocean (e.g. Bekker et al., 2008; Ader et al., 2009; Jiang et al., 2010; Swanson-Hysell et al., 2010). Although primary productivity in the Mesoproterozoic may have been lower than in later periods, the combination of redox stratification, limited upwelling, and reduced remineralization efficiency likely sustained an expanded deep-water DOC reservoir. However, whether the $\delta^{13}C_{org}$ gradient was globally pervasive or just a regional signature within the Yanliao basin, and whether the deep-water DOC pool was maintained throughout the whole of the mid-Proterozoic, requires further investigation.

5.3.2 Potential mechanism for short-term $\delta^{13}C$ perturbations

The short-term $\delta^{13}C_{carb}$ perturbations can be attributed to several mechanisms, including changes in organic carbon burial rate (Frank et al., 2003; Magaritz, 1989), water column stratification or overturning (Bartley et al., 1998), the influence of methane hydrates (Dickens et al., 1995; Kennedy et al., 2001), changes in primary productivity (Hoffman et al., 1998), or the oxidation of an oceanic organic carbon pool (Rothman et al., 2003; Fike et al., 2006; McFadden et al., 2008). Understanding how these factors interact with isotopic dynamics, particularly the relationship between $\delta^{13}C_{carb}$ and $\delta^{13}C_{org}$, can reveal more about the biogeochemical processes occurring within ancient marine environments.

In our study, four $\delta^{13}C_{carb}$ perturbations are identified, which roughly correspond to $\delta^{13}C_{org}$ changes, although their behavior is different across the basin, reflecting their distinct environmental setting and decoupling in $\delta^{13}C$ isotopic system. With the exception of the Qianxi section, all other sections show a $\delta^{13}C_{org}$ negative shift from ~-28‰ to ~-34‰ during or shortly after the N1 perturbation

446 (Fig.9). This pattern aligns with the start of a transgression event at the onset of Gaoyuzhuang Member
447 III, which marks the lithological boundary between members II and III, and we propose that this shift
448 in carbon isotope values reflects marine redox stratification that may have been driven by rising sea-
449 level. Consequently, following this event, the Kuancheng and Yanqing section would have been
450 situated below the chemocline, the mid-depth Jixian section may have been close to the chemocline,
451 and the Qianxi section would have remained above the chemocline, thus inducing an ~7‰ $\delta^{13}C_{org}$
452 gradient across the basin.

453 Following this, a pulsed negative $\delta^{13}C_{org}$ excursion reaching -30.6‰ is evident at ~88 m in the
454 Qianxi section, but $\delta^{13}C_{org}$ then rapidly returns to ~-26.17‰ at ~131 m (Fig. 4). We hypothesize that
455 this could be due to short-term upwelling from deeper anoxic waters to oxic surface waters, bringing
456 a more negative isotopic signal to the shallow waters. Nutrients may also have been transported from
457 deeper water, therefore further fueling surface primary productivity and increasing $\delta^{13}C_{org}$ values by
458 about 5‰ during the N2 interval in the Qianxi section, which may have created a favorable ecosystem
459 for the evolution of the large eukaryotes. This process would have likely deepened the chemocline due
460 to more oxygen generation in surface waters, thereby temporarily enhancing the decomposition of
461 part of the DOC pool in the mid-depth Jixian section, leading to the observed more negative $\delta^{13}C_{org}$
462 signature during the N2 interval in this section (Fig. 9C).

463 During the N3 interval, with the exception of the shallow water Qianxi section, a slight $\delta^{13}C_{org}$
464 negative perturbation is observed in other study sections, followed by a positive shift that correlates
465 with $\delta^{13}C_{carb}$ (Fig. 9). Specifically, $\delta^{13}C_{carb}$ values vary in magnitude during the negative excursion of the
466 N3 interval, with a difference of only ~-1.6‰ in the shallow Qianxi section, as opposed to >-3‰ in the
467 deeper sections, resulting in a ~2.5‰ gradient between the shallow- and deep- water for the $\delta^{13}C_{carb}$.

Several mechanisms could account for this observed gradient. One possibility is that carbonate platform weathering introduced heavier $\delta^{13}C$ signatures (~0‰) into nearshore areas, while upwelling of ^{13}C-depleted water from deep ocean in offshore area created a $\delta^{13}C_{DIC}$ gradient from proximal to distal environments (e.g. Melchin and Holmden, 2006; Shen et al., 2011). Alternatively, an enhanced biological pump could have contributed to the vertical $\delta^{13}C_{DIC}$ gradient. Oxygenic photosynthesis preferentially removes ^{12}C from surface DIC, enriching $\delta^{13}C_{DIC}$ in surface waters, while the export and remineralization of organic matter at depth release organic carbon, depleting $\delta^{13}C_{DIC}$ in deeper waters. Beyond a potentially intensified biological pump, increased deep-water oxygenation and the subsequent oxidation of the deep-water DOC pool could have led to further depletion of $\delta^{13}C_{DIC}$ at deep water, amplifying the surface-to-deep $\delta^{13}C_{DIC}$ gradient. During the N3 interval, persistently high sea levels would not have favored extensive carbonate platform weathering, making this mechanism less likely. While the biological pump may have played a role—supported by evidence of eukaryotic activity—the overall primary productivity during the early Mesoproterozoic remains uncertain and may have been buffered by the large DIC reservoir characteristic of this time. On the other hand, multiple redox proxies indicate a significant oxygenation event in deep waters during this period, including an increased I/(Ca+Mg) ratios in carbonate and a heavier $\delta^{98}Mo_{carb}$ trend, both suggesting intensified seafloor oxygenation (e.g. Shang et al., 2019; Luo et al., 2021; Xu et al., 2023). Therefore, while multiple factors may have contributed, the oxidation of the deep-water DOC pool likely played a primary role in driving the observed $\delta^{13}C_{carb}$ gradient during the N3 interval.

5.3.3 Oxygenation of the organic carbon pool in the early Mesoproterozoic ocean

Despite buffering of $\delta^{13}C_{carb}$ signatures by high pCO_2 and a large oceanic DIC pool during the early Mesoproterozoic (Grotzinger and Kasting, 1993; Bartley and Kah, 2004), our high-resolution carbon

490 isotope investigation of Member III of the Gaoyuzhuang Formation reveals a relatively dynamic carbon
491 cycle. To investigate the $\delta^{13}C_{DIC}$ gradient driven by the remineralization of the DOC pool in a strongly
492 redox-stratified ocean, we utilize a mass balance model that takes into account a large dissolved
493 organic carbon gradient between shallow and deeper waters.

494 The oceanic DIC reservoir in the modern ocean is estimated at approximately 3.2×10^{18} mol
495 (Holser et al., 1988). Given that it is estimated that pCO_2 levels during the early Mesoproterozoic were
496 10~100 times higher than the present level (Kasting, 1993), we assume the DIC reservoir during the
497 early Mesoproterozoic was at least 10 times larger than the modern reservoir size . This would have
498 resulted in significant buffering of $\delta^{13}C_{carb}$ changes (Bartley and Kah, 2004). On the other hand, the
499 DOC reservoir for the Neoproterozoic deep ocean has been estimated to be at least 10 times greater
500 than the modern DIC reservoir (Rothman et al., 2003), and we set a similar value for the
501 Mesoproterozoic deep ocean. During the Cretaceous period, the size of the deep-water carbon
502 reservoir was about 30 times larger than that of the shallow-water carbon reservoir (Kump, 1991).
503 Because of the longer residence time for deep oceanic DOC and very low primary productivity during
504 the Proterozoic (Rothman et al., 2003; Crockford et al., 2018), and also because TOC contents in deep
505 water sections were significantly higher than in shallow-water sediments, here we assume a steep
506 organic carbon gradient between the deep and shallow waters, with the size of the DOC reservoir in
507 the deep ocean being 100 times larger than in shallow waters. For the $\delta^{13}C$ composition of different
508 carbon reservoirs, at steady state, we assume the baseline $\delta^{13}C_{carb}$ composition to be -0.5‰ and its
509 gradient across the water depth was strongly buffered by the large DIC reservoir in the ocean. By
510 contrast, the $\delta^{13}C_{org}$ gradient is set at 10‰, with a value of -25‰ in shallow oxic waters controlled by
511 oxygenic photosynthesis, and a value of -35‰ in deep-water sediments, consistent with our data. The

512 estimates of carbon pool size and carbon isotopic composition for the early Mesoproterozoic ocean
513 are summarized in Table 1.

514 Although other impact factors could also influence the $\delta^{13}C_{DIC}$ compositions and gradient in the
515 water column (e.g., biological pump, upwelling, and pCO_2 changes), our mass-balance mixing model
516 highlights the significant impact of both DOC remineralization rates and gradients in the size and
517 isotopic composition of the DOC pool on $\delta^{13}C_{DIC}$ differences during the early Mesoproterozoic (Fig. 11).
518 The $\delta^{13}C_{DIC}$ gradient remains highly buffered when the remineralization rate is limited, displaying little
519 $\delta^{13}C_{DIC}$ variation between shallow and deeper water. However, the high remineralization rates
520 substantially decrease the $\delta^{13}C_{DIC}$ compositions, leading to a pronounced gradient across the water
521 depth. This suggests that a larger organic carbon remineralization flux can induce significant $\delta^{13}C_{DIC}$
522 differences, even in an ocean with a large DIC pool (Bartley and Kah, 2004). On the other hand, in
523 shallow waters, the $\delta^{13}C_{DIC}$ gradient remains negligible, even under high remineralization rates. This
524 suggests that the shallow water DIC reservoir is relatively stable, possibly due to the lower overall size
525 of the DOC pool and smaller differences between carbon isotopic systems ($\Delta^{13}C$) in these settings.
526 However, in deeper waters, the $\delta^{13}C_{DIC}$ composition is much more sensitive to changes in
527 remineralization rates, likely driven by the larger DOC reservoir and more negative $\delta^{13}C_{DOC}$ values.
528 These results indicate that the carbon cycle in the deep Mesoproterozoic ocean would have been
529 particularly responsive to variability in DOC remineralization, which would have strongly influenced
530 the isotopic composition of the deep water DIC pool.

531 This differential response to the generation of a $\delta^{13}C_{carb}$ gradient between shallow and deeper
532 waters aligns well with $\delta^{13}C_{carb}$ data for the N3 interval (Fig. 9A). To achieve a $\delta^{13}C_{carb}$ gradient of ~2.5‰
533 between the shallow and deep-water reservoir, as observed in our data, approximately 8% of the DOC

pool would need to be oxidized in the deep ocean (Fig. 11). Although sulfate might act as an oxidant in deep-water environment, sulfate in the ocean sourced from weathering during the time remains lower, in particular in the distal deeper water basin. Therefore, we prefer an oxygen-driven oxidation model supplied from surface waters by oxygenic photosynthesis. Since the oxidation of 1 mol of carbon requires 1 mol of O_2, the remineralization of 8% deep water DOC would consume 2.56×10^{18} mol oxygen (giving O_2 is the main oxidant). This oxygen flux is equal to the amount of approximately 7% of the present atmospheric oxygenation concentration (Keeling et al., 1993). The oxygen level during the early Mesoproterozoic has been estimated using several geochemical proxies (e.g. Ce/Ce* anomalies in shallow water carbonates and Cr isotopic fractionations in shales), providing a wide range of variability and uncertainties, from less than 0.1% to 4~8% PAL (Planavsky et al., 2014; Canfield et al., 2018; Liu et al., 2021; Xie et al., 2023). This has led to considerable debate over whether low oxygen levels limited the early evolution of eukaryotes (e.g., Planavsky et al., 2014; Canfield et al., 2018).

Our estimate suggests that environmental oxygenation may have supported the evolution of early multicellular eukaryotes in the early Meosproterozoic ocean. The episodic oxygenation events may have dropped the redox chemocline and helped to create more widespread and favorable conditions for the growth and diversification of early eukaryotes by enhancing nutrient availability and increasing organic carbon remineralization rates in shallow, oxic waters. These environmental changes likely contributed to the enlargement of body size and the greater morphological complexity observed in eukaryotic fossils from this time period.

Conclusions

Our high-resolution carbon isotope analyses across members III and IV of the Gaoyuzhuang

555 Formation allow us to identify chemostratigraphic correlations between sections deposited across the
556 basin, and also provides new insight into the behavior of the carbon cycle in the early Mesoproterozoic
557 redox-stratified ocean. While $\delta^{13}C_{carb}$ profiles exhibit a narrow range, we recognize four discrete $\delta^{13}C_{carb}$
558 perturbations. This chemostratigraphic framework combines the sedimentary cycles to calibrate the
559 chronological sequence of the macroscopic eukaryotic evolution and oxygenation events and to build
560 up reliable $\delta^{13}C_{carb}$ curves for the shallow and deeper-water facies in the early Mesoproterozoic ocean.

561 Our $\delta^{13}C$ analyses also reveal a large $\delta^{13}C_{org}$ gradient (reaching ~7‰) across the basin, indicating
562 a decoupling in the carbon isotopic system between shallow and deep waters, likely influenced by
563 microbial communities in a redox-stratified ocean. Additionally, an ~2.5‰ $\delta^{13}C_{carb}$ gradient during the
564 N3 perturbation points to redox changes as the driving mechanism. Mass balance modeling simulates
565 the effect of a hypothetical oxygenation event leading to the remineralization of the deep-ocean DOC
566 reservoir. The result indicates approximately 8% of the deep-water DOC pool needed to be oxidized to
567 induce the observed $\delta^{13}C_{carb}$ gradient, which would consume oxygen equivalent to about 7% of the
568 modern atmospheric O_2 concentration. Thus, our research not only provides insight into the dynamic
569 nature of the oceanic carbon cycle during the early Mesoproterozoic, but also offers strong evidence
570 of the positive impact of environmental oxygenation on early eukaryote evolution.

571 **Acknowledgements**

572 This work was supported by the National Key Research and Development Program of China
573 (2022YFF0800100), the National Natural Science Foundation of China (42472048). SWP acknowledges
574 support from the World Research Hub (WRH) Program of the International Research Frontiers Initiative,
575 Tokyo Institute of Technology. We thank Dr. Chengguo Guan for sample preparation and organic carbon

isotope analysis and Dr. Jing Liu for carbonate carbon isotope analysis. We sincerely appreciate the two reviewers and the editor for their valuable comments and improvements to this paper.

References

Ader, M., Macouin, M., Trindade, R.I.F., Hadrien, M.-H., Yang, Z., Sun, Z., Besse, J., 2009. A multilayered water column in the Ediacaran Yangtze platform? Insights from carbonate and organic matter paired δ13C. Earth and Planetary Science Letters 288, 213–227. https://doi.org/10.1016/j.epsl.2009.09.024

Ahm, A.-S., Husson, J., 2022. Local and Global Controls on Carbon Isotope Chemostratigraphy, Elements in Geochemical Tracers in Earth System Science. Cambridge University Press, Cambridge. https://doi.org/10.1017/9781009028882

Banner, J.L., Hanson, G.N., 1990. Calculation of simultaneous isotopic and trace element variations during water-rock interaction with applications to carbonate diagenesis. Geochimica et Cosmochimica Acta 54, 3123–3137. https://doi.org/10.1016/0016-7037(90)90128-8

Bartley, J., Pope, M., Knoll, A., Petrov, P., Semikhatov, M., Sergeev, V., 1998. A Precambrian-Cambrian boundary succession from the western Siberian platform: Geochemistry, stratigraphy, and paleontology. Geological Magazine 135, 473–494.

Bartley, J.K., Kah, L.C., 2004. Marine carbon reservoir, Corg-Ccarb coupling, and the evolution of the Proterozoic carbon cycle. Geology 32, 129–132. https://doi.org/10.1130/G19939.1

Bekker, A., Holmden, C., Beukes, N.J., Kenig, F., Eglinton, B., Patterson, W.P., 2008. Fractionation between inorganic and organic carbon during the Lomagundi (2.22–2.1 Ga) carbon isotope excursion. Earth and Planetary Science Letters 271, 278–291. https://doi.org/10.1016/j.epsl.2008.04.021

Bekker, A., Kaufman, A.J., 2007. Oxidative forcing of global climate change: A biogeochemical record across the oldest Paleoproterozoic ice age in North America. Earth and Planetary Science Letters 258, 486–499. https://doi.org/10.1016/j.epsl.2007.04.009

Brand, U., Veizer, J., 1981. Chemical diagenesis of a multicomponent carbonate system; 2, Stable isotopes. Journal of Sedimentary Research 51, 987–997. https://doi.org/10.1306/212F7DF6-2B24-11D7-8648000102C1865D

Brasier, M.D., Lindsay, J.F., 1998. A billion years of environmental stability and the emergence of eukaryotes: New data from northern Australia. Geology 26, 555–558. https://doi.org/10.1130/0091-7613(1998)026<0555:ABYOES>2.3.CO;2

Buick, R., Des Marais, D.J., Knoll, A.H., 1995. Stable isotopic compositions of carbonates from the Mesoproterozoic Bangemall group, northwestern Australia. Chemical Geology 123, 153–171. https://doi.org/10.1016/0009-2541(95)00049-R

Canfield, D.E., Zhang, S., Frank, A.B., Wang, X., Wang, H., Su, J., Ye, Y., Frei, R., 2018. Highly fractionated chromium isotopes in Mesoproterozoic-aged shales and atmospheric oxygen. Nature Communications 9, 2871. https://doi.org/10.1038/s41467-018-05263-9

Chen, K., Miao, L., Zhao, F., Zhu, M., 2023. Carbonaceous macrofossils from the early Mesoproterozoic Gaoyuzhuang Formation in the Yanshan Range, North China. Precambrian Research 392, 107074. https://doi.org/10.1016/j.precamres.2023.107074

Chen, K., Yang, C., Miao, L., Zhao, F., Zhu, M., 2024. New SIMS U–Pb zircon age on the macroscopic multicellular eukaryotes from the early Mesoproterozoic Gaoyuzhuang Formation, North China. Geological Magazine 161, e2. https://doi.org/10.1017/S0016756824000220

Chu, X., Zhang, T., Zhang, Q., Lyons, T.W., 2007. Sulfur and carbon isotope records from 1700 to 800Ma carbonates of the Jixian section, northern China: Implications for secular isotope variations in Proterozoic seawater and relationships to global supercontinental events. Geochimica et Cosmochimica Acta 71, 4668–4692. https://doi.org/10.1016/j.gca.2007.07.017

Crockford, P.W., Hayles, J.A., Bao, H., Planavsky, N.J., Bekker, A., Fralick, P.W., Halverson, G.P., Bui, T.H., Peng, Y., Wing, B.A., 2018. Triple oxygen isotope evidence for limited mid-Proterozoic primary productivity. Nature 559, 613–616. https://doi.org/10.1038/s41586-018-0349-y

Deuser, W.G., 1970. Carbon-13 in Black Sea Waters and Implications for the Origin of Hydrogen Sulfide. Science 168, 1575–1577. https://doi.org/10.1126/science.168.3939.1575

Dickens, G.R., O'Neil, J.R., Rea, D.K., Owen, R.M., 1995. Dissociation of oceanic methane hydrate as a cause of the carbon isotope excursion at the end of the Paleocene. Paleoceanography 10, 965–971. https://doi.org/10.1029/95PA02087

Fang, H., Tang, D., Shi, X., Zhou, L., Zhou, X., Wu, M., Song, H., Riding, R., 2022. Early Mesoproterozoic Ca-carbonate precipitates record fluctuations in shallow marine oxygenation. Precambrian Research 373, 106630. https://doi.org/10.1016/j.precamres.2022.106630

Fike, D.A., Grotzinger, J.P., Pratt, L.M., Summons, R.E., 2006. Oxidation of the Ediacaran Ocean. Nature 444, 744–747. https://doi.org/10.1038/nature05345

Frank, T.D., Kah, L.C., Lyons, T.W., 2003. Changes in organic matter production and accumulation as a mechanism for isotopic evolution in the Mesoproterozoic ocean. Geological Magazine 140, 397–420. https://doi.org/10.1017/S0016756803007830

Fry, B., Jannasch, H.W., Molyneaux, S.J., Wirsen, C.O., Muramoto, J.A., King, S., 1991. Stable isotope studies of the carbon, nitrogen and sulfur cycles in the Black Sea and the Cariaco Trench. Deep Sea Research Part A. Oceanographic Research Papers 38, S1003–S1019. https://doi.org/10.1016/S0198-0149(10)80021-4

Galimov, E.M., 2004. The pattern of δ13Corg versus HI/OI relation in recent sediments as an indicator of geochemical regime in marine basins: comparison of the Black Sea, Kara Sea, and Cariaco Trench. Chemical Geology 204, 287–301. https://doi.org/10.1016/j.chemgeo.2003.11.014

Gong, C., Hollander, D.J., 1997. Differential contribution of bacteria to sedimentary organic matter in oxic and anoxic environments, Santa Monica Basin, California. Organic Geochemistry 26, 545–563. https://doi.org/10.1016/S0146-6380(97)00018-1

Grotzinger, J.P., Kasting, J.F., 1993. New Constraints on Precambrian Ocean Composition. The Journal of Geology 101, 235–243.

Guo, H., Du, Y., Kah, L.C., Huang, J., Hu, C., Huang, H., Yu, W., 2013. Isotopic composition of organic and inorganic carbon from the Mesoproterozoic Jixian Group, North China: Implications for biological and oceanic evolution. Precambrian Research 224, 169–183. https://doi.org/10.1016/j.precamres.2012.09.023

Hayes, J.M., Strauss, H., Kaufman, A.J., 1999. The abundance of 13C in marine organic matter and isotopic fractionation in the global biogeochemical cycle of carbon during the past 800 Ma. Chemical Geology 161, 103–125. https://doi.org/10.1016/S0009-2541(99)00083-2

Hinrichs, K.-U., Summons, R.E., Orphan, V., Sylva, S.P., Hayes, J.M., 2000. Molecular and isotopic analysis of anaerobic methane-oxidizing communities in marine sediments. Organic

660 Geochemistry 31, 1685–1701. https://doi.org/10.1016/S0146-6380(00)00106-6
661 Hoffman, P.F., Kaufman, A.J., Halverson, G.P., Schrag, D.P., 1998. A Neoproterozoic Snowball Earth.
662 Science 281, 1342–1346. https://doi.org/10.1126/science.281.5381.1342
663 Hollander, D.J., McKenzie, J.A., 1991. CO2 control on carbon-isotope fractionation during aqueous
664 photosynthesis: A paleo-pCO2 barometer. Geology 19, 929–932.
665 https://doi.org/10.1130/0091-7613(1991)019<0929:CCOCIF>2.3.CO;2
666 Hollander, D.J., Smith, M.A., 2001. Microbially mediated carbon cycling as a control on the δ13C of
667 sedimentary carbon in eutrophic Lake Mendota (USA): new models for interpreting isotopic
668 excursions in the sedimentary record. Geochimica et Cosmochimica Acta 65, 4321–4337.
669 https://doi.org/10.1016/S0016-7037(00)00506-8
670 Holser, W.T., Schidlowski, M., Mackenzie, F., Maynard, J., 1988. Biogeochemical Cycles of Carbon and
671 Sulfur. pp. 105–174.
672 Hotinski, R.M., Kump, L.R., Arthur, M.A., 2004. The effectiveness of the Paleoproterozoic biological
673 pump: A δ13C gradient from platform carbonates of the Pethei Group (Great Slave Lake
674 Supergroup, NWT). GSA Bulletin 116, 539–554. https://doi.org/10.1130/B25272.1
675 Jiang, G., Wang, X., Shi, X., Zhang, S., Xiao, S., Dong, J., 2010. Organic carbon isotope constraints on the
676 dissolved organic carbon (DOC) reservoir at the Cryogenian–Ediacaran transition. Earth and
677 Planetary Science Letters 299, 159–168. https://doi.org/10.1016/j.epsl.2010.08.031
678 Jin, S., Ma, P., Guo, H., Yu, W., Xu, L., Lin, Q., 2022. Genesis of Mesoproterozoic Gaoyuzhuang Formation
679 Manganese Ore in Qinjiayu, East Hebei: Constraints from Mineralogical and Geochemical
680 Evidences. Earth Science-Journal of China University of Geosciences 47, 277–289.
681 https://doi.org/10.3799/dqkx.2021.055
682 Johnston, D.T., Macdonald, F.A., Gill, B.C., Hoffman, P.F., Schrag, D.P., 2012. Uncovering the
683 Neoproterozoic carbon cycle. Nature 483, 320–323. https://doi.org/10.1038/nature10854
684 Karl, D.M., Knauer, G.A., 1991. Microbial production and particle flux in the upper 350 m of the Black
685 Sea. Deep Sea Research Part A. Oceanographic Research Papers 38, S921–S942.
686 https://doi.org/10.1016/S0198-0149(10)80017-2
687 Kasting, J.F., 1993. Earth's Early Atmosphere. Science 259, 920–926.
688 https://doi.org/10.1126/science.11536547
689 Keeling, R.F., Najjar, R.P., Bender, M.L., Tans, P.P., 1993. What atmospheric oxygen measurements can
690 tell us about the global carbon cycle. Global Biogeochemical Cycles 7, 37–67.
691 Kennedy, M.J., Christie-Blick, N., Sohl, L.E., 2001. Are Proterozoic cap carbonates and isotopic
692 excursions a record of gas hydrate destabilization following Earth's coldest intervals? Geology
693 29, 443–446. https://doi.org/10.1130/0091-7613(2001)029<0443:APCCAI>2.0.CO;2
694 Knoll, A.H., Hayes, J.M., Kaufman, A.J., Swett, K., Lambert, I.B., 1986. Secular variation in carbon
695 isotope ratios from Upper Proterozoic successions of Svalbard and East Greenland. Nature 321,
696 832–838. https://doi.org/10.1038/321832a0
697 Kroopnick, P., 1974. The dissolved O2-CO2-13C system in the eastern equatorial pacific. Deep Sea
698 Research and Oceanographic Abstracts 21, 211–227. https://doi.org/10.1016/0011-
699 7471(74)90059-X
700 Kroopnick, P.M., 1985. The distribution of 13C of ΣCO2 in the world oceans. Deep Sea Research Part A.
701 Oceanographic Research Papers 32, 57–84. https://doi.org/10.1016/0198-0149(85)90017-2
702 Kump, L.R., 1991. Interpreting carbon-isotope excursions: Strangelove oceans. Geology 19, 299–302.
703 https://doi.org/10.1130/0091-7613(1991)019<0299:ICIESO>2.3.CO;2

Kump, L.R., Arthur, M.A., 1999. Interpreting carbon-isotope excursions: carbonates and organic matter. Chemical Geology 161, 181–198. https://doi.org/10.1016/S0009-2541(99)00086-8

Li, D., Zhang, Xiaolin, Hu, D., Chen, X., Huang, W., Zhang, Xu, Li, M., Qin, L., Peng, S., Shen, Y., 2018. Evidence of a large δ13Ccarb and δ13Corg depth gradient for deep-water anoxia during the late Cambrian SPICE event. Geology 46, 631–634. https://doi.org/10.1130/G40231.1

Li, H., Zhu, S., Xiang, Z., Su, W., Lu, S., Zhou, H., Geng, J., Li, S., Yang, F., 2010. Zircon U-Pb dating on tuff bed from Gaoyuzhuang Formation in Yanqing, Beijing: Further constraints on the new subdivision of the Mesoproterozoic stratigraphy in the northern North China Craton. Acta Petrologica Sinica 7, 2131–2140.

Liu, G., Zhang, S., Li, H., Bao, X., Zhao, H., Liang, D., Wu, H., Tang, D., Zhu, X., Yang, T., 2022. Cyclostratigraphic calibration of the ca. 1.56 Ga carbon isotope excursion and oxygenation event recorded in the Gaoyuzhuang Formation, north China. Global and Planetary Change 216, 103916. https://doi.org/10.1016/j.gloplacha.2022.103916

Liu, Y., Zhao, M., He, T., Li, X., Poulton, S.W., 2023. Formation of molar tooth structures in low sulfate Precambrian oceans. Geochimica et Cosmochimica Acta 354, 62–73. https://doi.org/10.1016/j.gca.2023.06.013

Lu, S., Zhao, G., Wang, H., Hao, G., 2008. Precambrian metamorphic basement and sedimentary cover of the North China Craton: A review. Precambrian Research 160, 77–93. https://doi.org/10.1016/j.precamres.2007.04.017

Luo, G., Junium, C.K., Kump, L.R., Huang, J., Li, C., Feng, Q., Shi, X., Bai, X., Xie, S., 2014. Shallow stratification prevailed for ~1700 to ~1300 Ma ocean: Evidence from organic carbon isotopes in the North China Craton. Earth and Planetary Science Letters 400, 219–232. https://doi.org/10.1016/j.epsl.2014.05.020

Luo, J., Long, X., Bowyer, F.T., Mills, B.J.W., Li, J., Xiong, Y., Zhu, X., Zhang, K., Poulton, S.W., 2021. Pulsed oxygenation events drove progressive oxygenation of the early Mesoproterozoic ocean. Earth and Planetary Science Letters 559, 116754. https://doi.org/10.1016/j.epsl.2021.116754

Magaritz, M., 1989. 13C minima follow extinction events: A clue to faunal radiation. Geology 17, 337–340. https://doi.org/10.1130/0091-7613(1989)017<0337:CMFEEA>2.3.CO;2

McFadden, K.A., Huang, J., Chu, X., Jiang, G., Kaufman, A.J., Zhou, C., Yuan, X., Xiao, S., 2008. Pulsed oxidation and biological evolution in the Ediacaran Doushantuo Formation. Proceedings of the National Academy of Sciences 105, 3197–3202. https://doi.org/10.1073/pnas.0708336105

Melchin, M.J., Holmden, C., 2006. Carbon isotope chemostratigraphy in Arctic Canada: Sea-level forcing of carbonate platform weathering and implications for Hirnantian global correlation. Palaeogeography, Palaeoclimatology, Palaeoecology 234, 186–200. https://doi.org/10.1016/j.palaeo.2005.10.009

Oehlert, A.M., Lamb-Wozniak, K.A., Devlin, Q.B., Mackenzie, G.J., Reijmer, J.J.G., Swart, P.K., 2012. The stable carbon isotopic composition of organic material in platform derived sediments: implications for reconstructing the global carbon cycle. Sedimentology 59, 319–335. https://doi.org/10.1111/j.1365-3091.2011.01273.x

Planavsky, N.J., Reinhard, C.T., Wang, X., Thomson, D., McGoldrick, P., Rainbird, R.H., Johnson, T., Fischer, W.W., Lyons, T.W., 2014. Low Mid-Proterozoic atmospheric oxygen levels and the delayed rise of animals. Science 346, 635–638. https://doi.org/10.1126/science.1258410

Qiao, X., Gao, L., 2007. Mesoproterozoic palaeoearthquake and palaeogeography in Yan-Liao Aulacogen. Journal of Palaeogeography 9, 337–352.

Retallack, G.J., Chen, Z.-Q., Huang, Y., Fang, Y., 2021. Oxidizing atmosphere and life on land during the late Paleoproterozoic outset of the “boring billion.” Precambrian Research 364, 106361. https://doi.org/10.1016/j.precamres.2021.106361

Romanek, C.S., Grossman, E.L., Morse, J.W., 1992. Carbon isotopic fractionation in synthetic aragonite and calcite: Effects of temperature and precipitation rate. Geochimica et Cosmochimica Acta 56, 419–430. https://doi.org/10.1016/0016-7037(92)90142-6

Rothman, D.H., Hayes, J.M., Summons, R.E., 2003. Dynamics of the Neoproterozoic carbon cycle. Proceedings of the National Academy of Sciences 100, 8124–8129. https://doi.org/10.1073/pnas.0832439100

Selden, P.A., Edwards, D., 1989. Colonisation of the land, in: Evolution and the Fossil Record. pp. 122–152.

Shang, M., Tang, D., Shi, X., Zhou, L., Zhou, X., Song, H., Jiang, G., 2019. A pulse of oxygen increase in the early Mesoproterozoic ocean at ca. 1.57–1.56 Ga. Earth and Planetary Science Letters 527, 115797. https://doi.org/10.1016/j.epsl.2019.115797

Shen, B., Xiao, S., Bao, H., Kaufman, A.J., Zhou, C., Yuan, X., 2011. Carbon, sulfur, and oxygen isotope evidence for a strong depth gradient and oceanic oxidation after the Ediacaran Hankalchough glaciation. Geochimica et Cosmochimica Acta 75, 1357–1373. https://doi.org/10.1016/j.gca.2010.12.015

Shen, Y., Zhang, T., Chu, X., 2005. C-isotopic stratification in a Neoproterozoic postglacial ocean. Precambrian Research 137, 243–251. https://doi.org/10.1016/j.precamres.2005.03.004

Surge, D.M., Savarese, M., Robert Dodd, J., Lohmann, K.C., 1997. Carbon isotopic evidence for photosynthesis in Early Cambrian oceans. Geology 25, 503–506. https://doi.org/10.1130/0091-7613(1997)025<0503:CIEFPI>2.3.CO;2

Swanson-Hysell, N.L., Rose, C.V., Calmet, C.C., Halverson, G.P., Hurtgen, M.T., Maloof, A.C., 2010. Cryogenian Glaciation and the Onset of Carbon-Isotope Decoupling. Science 328, 608–611. https://doi.org/10.1126/science.1184508

Swart, P.K., Oehlert, A.M., 2018. Revised interpretations of stable C and O patterns in carbonate rocks resulting from meteoric diagenesis. Sedimentary Geology 364, 14–23. https://doi.org/10.1016/j.sedgeo.2017.12.005

Tian, H., Jian, Z., Li, H., Su, W., Zhou, H.-Y., Yang, L.-G., Xiang, Z.-Q., Geng, J.-Z., Liu, H., Zhu, S.-X., Xu, Z.-Q., 2015. Zircon LA-MC-ICPMS U-Pb dating of tuff from mesoproterozoic Gaoyuzhuang Formation in Jixian County of North China and its geological significance. Acta Geoscientica Sinica 36, 647–658. https://doi.org/10.3975/cagsb.2015.05.12

Werne, J.P., Hollander, D.J., 2004. Balancing supply and demand: controls on carbon isotope fractionation in the Cariaco Basin (Venezuela) Younger Dryas to present. Marine Chemistry 92, 275–293. https://doi.org/10.1016/j.marchem.2004.06.031

Xu, D., Qin, Z., Wang, X., Li, J., Shi, X., Tang, D., Liu, J., 2023. Extensive sea-floor oxygenation during the early Mesoproterozoic. Geochimica et Cosmochimica Acta 354, 186–196. https://doi.org/10.1016/j.gca.2023.06.007

Yoshinaga, M.Y., Holler, T., Goldhammer, T., Wegener, G., Pohlman, J.W., Brunner, B., Kuypers, M.M.M., Hinrichs, K.-U., Elvert, M., 2014. Carbon isotope equilibration during sulphate-limited anaerobic oxidation of methane. Nature Geoscience 7, 190–194. https://doi.org/10.1038/ngeo2069

Zhang, K., Zhu, X., Wood, R.A., Shi, Y., Gao, Z., Poulton, S.W., 2018. Oxygenation of the Mesoproterozoic

ocean and the evolution of complex eukaryotes. Nature Geoscience 11, 345–350. https://doi.org/10.1038/s41561-018-0111-y

Zhu, S., Li, H., Sun, L., Liu, H., 2022. Meso-Neoproterozoic Stratigraphic Sequences in the Yanliao Faulted-Depression Zone, North China Craton, in: Wang, T. (Ed.), Meso-Neoproterozoic Geology and Petroleum Resources in China. Springer Nature Singapore, Singapore, pp. 47–89. https://doi.org/10.1007/978-981-19-5666-9_2

Zhu, S., Zhu, M., Knoll, A.H., Yin, Z., Zhao, F., Sun, S., Qu, Y., Shi, M., Liu, H., 2016. Decimetre-scale multicellular eukaryotes from the 1.56-billion-year-old Gaoyuzhuang Formation in North China. Nature Communications 7, 11500. https://doi.org/10.1038/ncomms11500

803 **Table**

804 Table 1. Estimated carbon pool size and carbon isotopic composition for the early Mesoproterozoic

805 ocean.

	Shallow water	Deep water
DIC size	32×10^{18} mol	32×10^{18} mol
$\delta^{13}C_{DIC}$	-0.5‰	-0.5‰
DOC size	0.32×10^{18} mol	32×10^{18} mol
$\delta^{13}C_{DOC}$	-25‰	-35‰
Present DIC size	32×10^{18} mol[1]	
Modern atmospheric O_2	37×10^{18} mol[2]	
Mass balance formula	$\delta^{13}C_{DIC,m} = (\delta^{13}C_{DIC,0} \times M_{DIC,0}) + (\delta^{13}C_{DOC,0} \times M_{DOC,oxidzed})/(M_{DIC,0} + M_{DOC,oxidzed})$	

806 *1. Cited from (Holser et al., 1988); 2.Cited from (Keeling et al., 1993).

807

Figures

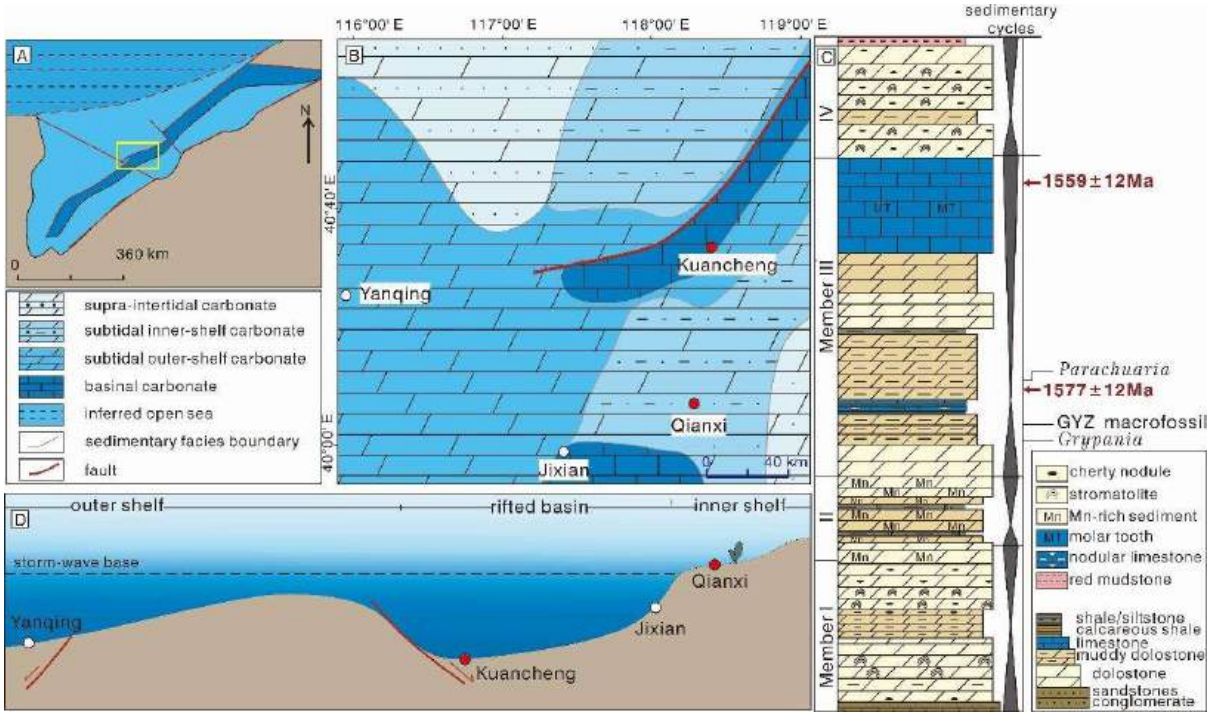

Figure 1. Paleogeographic maps and cross-section showing the study sites, with generalized stratigraphy of the Gaoyuzhuang Formation. A. Simplified paleogeographic map of the Yanliao area, North China craton, during the early Mesoproterozoic (modified after Qiao and Gao, 2007). B. Detailed paleogeographic and sedimentary facies of the study area (modified after Jin et al., 2022). The red circles represent the location of the sections analyzed in this study; open circles indicate other sections discussed in this paper. C. General stratigraphic column of the Gaoyuzhuang Formation with sedimentary cycles, where the apex of the triangles represents deepening water depth. The stratigraphic column refers to the stratotype section at Jixian. The age constraints are from the Jixian section (Li et al., 2010) and the Yanqing section (Tian et al., 2015). The fossil records are adopted from Zhu et al. (2016) and Chen et al. (2023). D. Inferred sedimentary settings of the study sections during deposition of Gaoyuzhuang Member III.

Figure 2. Lithologies and sedimentary structures in the Gaoyuzhuang Formation at the Qianxi section. A. Storm-agitated deformation structures in the lower part of Member III. Yellow lines highlight the hummocky cross-stratification and leaf-shaped calcareous structures associated with storm deposits. B. Macrofossil hosting horizon. Red lines mark the two layers of muddy dolostones preserving the Gaoyuzhuang macrofossils. C. Stromatolites of Gaoyuzhuang Member IV. D. Cherty concretions and banded chert in the upper part of Gaoyuzhuang Member IV.

Figure 3. Lithologies and sedimentary structures in the Gaoyuzhuang Formation at the Kuancheng section. A. Mn-rich banded dolostone in the upper part of Member II. The manganese is enriched in silty bands. B. Eukaryotic fossil fragments preserved in organic-rich calcareous shales in the lower part of Member III (mark by red lines). C. Nodular limey dolostone intercalated with limey mudstones and shales in the lower part of Member III. D. Medium – thin bedded limy dolostones with sedimentary rhythm in lower Member III .

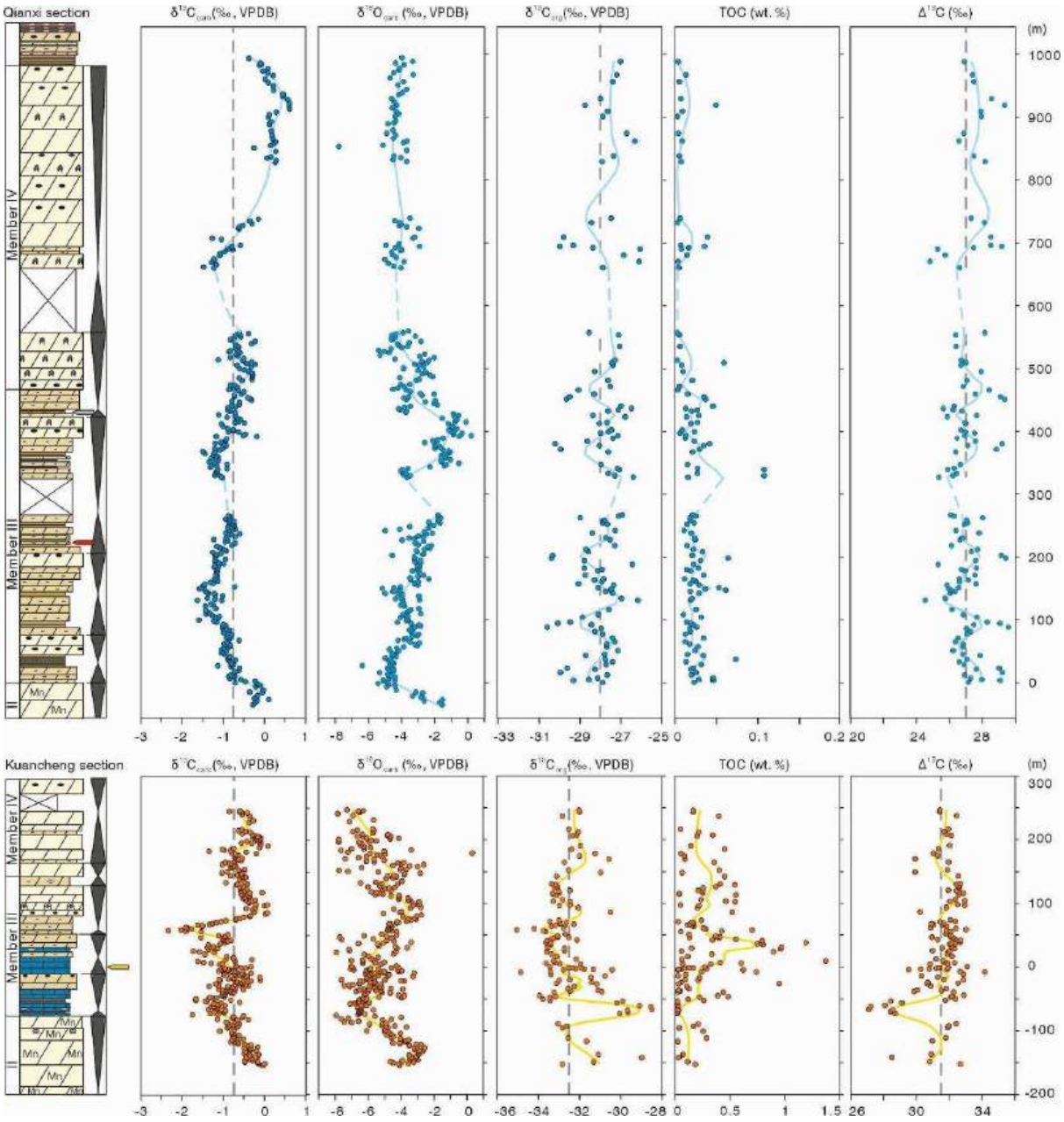

836

837 **Figure 4. Carbon-oxygen isotope and TOC concentration profiles of the Qianxi and Kuancheng**

838 **sections.** $\Delta^{13}C$ represents the isotopic difference between $\delta^{13}C_{carb}$ and $\delta^{13}C_{org}$. Arrows denote fossil-

839 bearing horizons: red arrows mark in-situ, decimeter-sized macrofossils (Zhu et al., 2016); yellow

840 arrows denote macrofossil fragments preserved in the Kuancheng section (Zhu et al., 2016); and the

841 grey arrow indicates a centimeter-scale fossil (Chen et al., 2023). A detailed lithological overview and

842 high-resolution results for the middle fossil-bearing horizon in the Qianxi section (marked by a red

arrow) are shown in Figure 3. The grey vertical dashed lines represent the average values for $\delta^{13}C_{carb}$, $\delta^{13}C_{org}$, and $\Delta^{13}C$. Blue and yellow curves represent LOESS-smoothed lines. See Figure 1 for the lithological key.

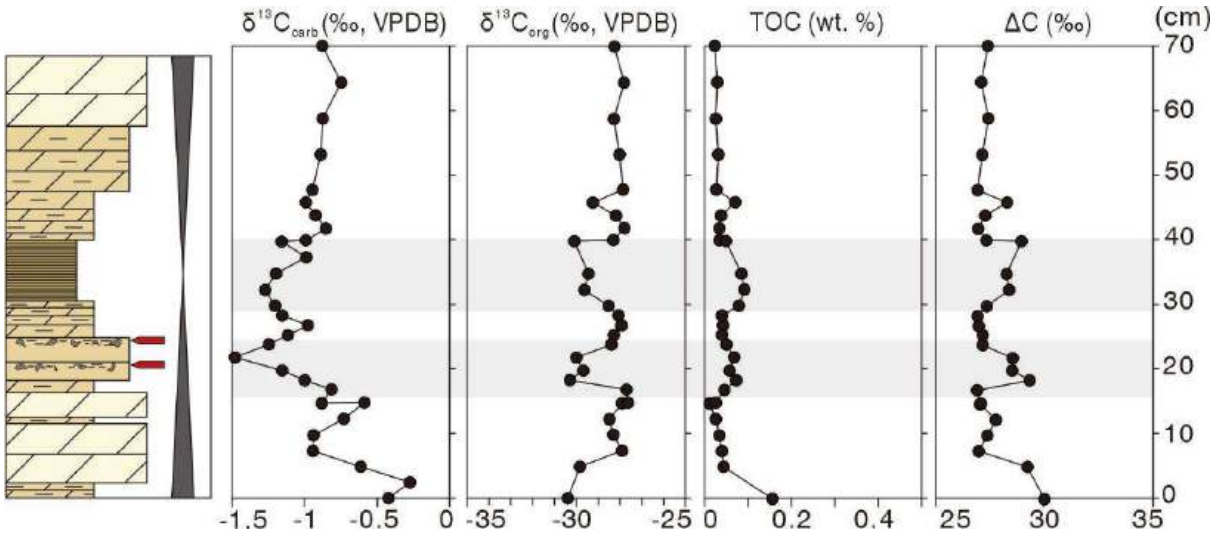

Figure 5. Isotopic and geochemical profiles through the main macrofossil-hosting horizon in the Qianxi section. The grey shading shows samples with relative higher TOC (>0.05 wt. %), and lower $\delta^{13}C_{carb}$ and $\delta^{13}C_{org}$. The red arrows mark the positions of fossil preservation. See Fig. 1 for lithological key.

853 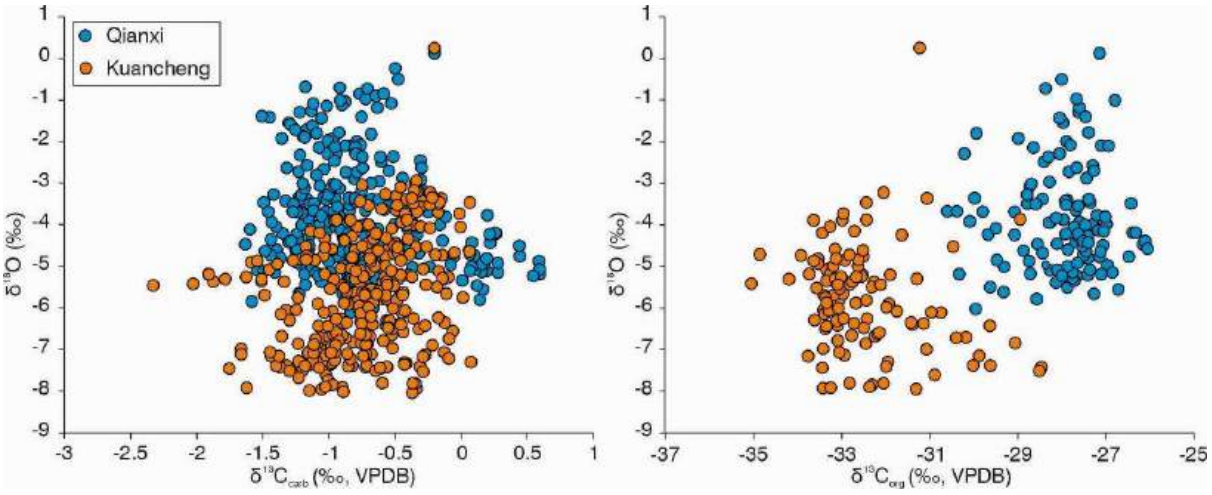

854 **Figure 6. Cross plots of $\delta^{18}O_{carb}$ vs. $\delta^{13}C_{carb}$ (left) and $\delta^{18}O_{carb}$ vs. $\delta^{13}C_{org}$ (right).** Blue circles: Qianxi

855 samples; Orange circles: Kuancheng samples. San

856

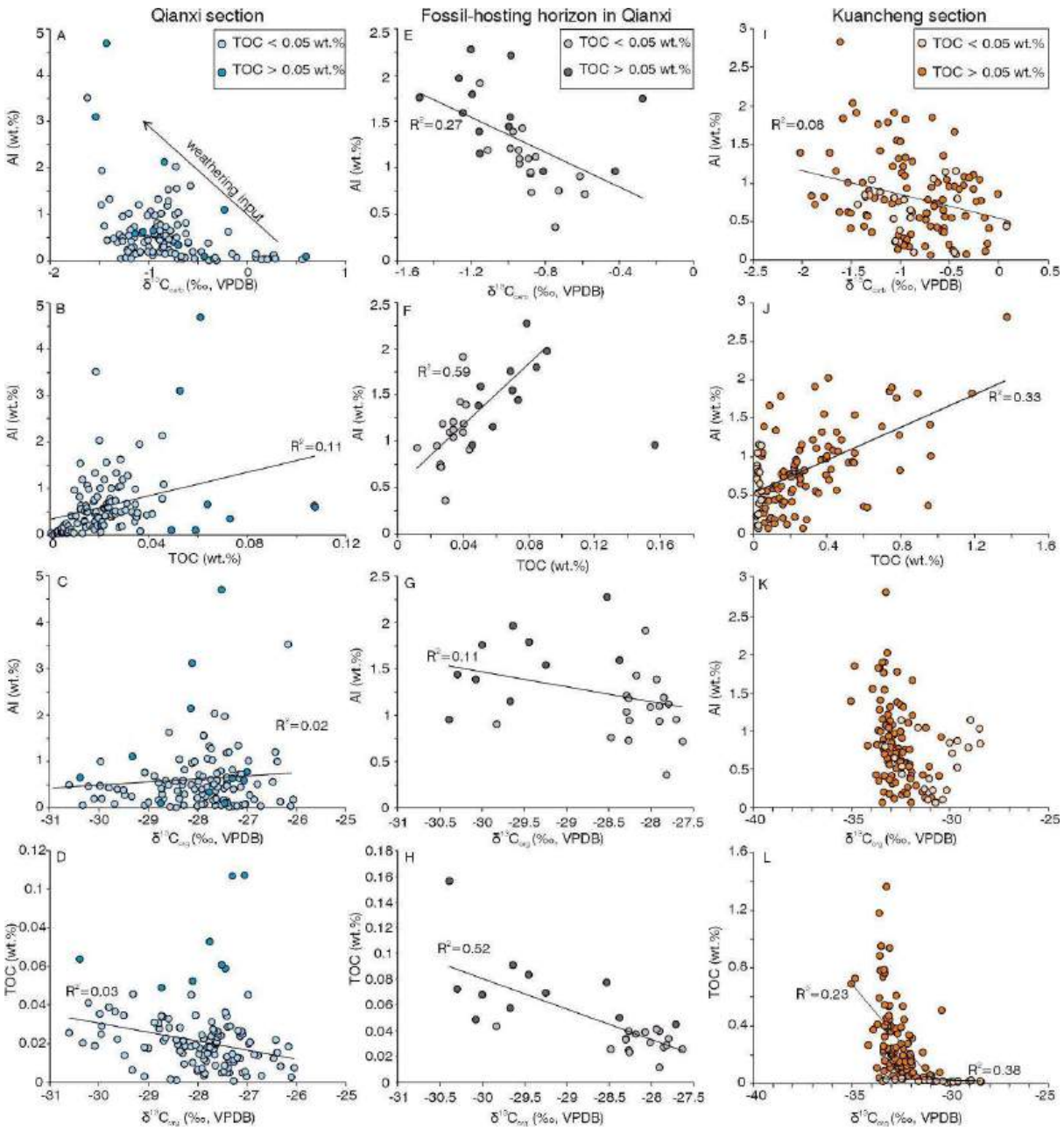

857

858 **Figure 7. Evaluation of the influence of detrital inputs on the carbon isotope system of Gaoyuzhuang**

859 **carbonates.** Qianxi section samples (A – D): A. Cross-plot of Al vs. $\delta^{13}C_{carb}$, where only a few samples

860 with high Al contents have the most negative $\delta^{13}C_{carb}$ values. B. Cross-plot of Al and TOC, showing a

861 very weak correlation. C. Cross-plot of Al vs. $\delta^{13}C_{org}$, showing no significant correlation. D. Cross-plot of

862 TOC vs. $\delta^{13}C_{org}$, showing no significant correlation. In-situ fossil-hosting interval of the Qianxi section

863 (E - H): E. Slight correlation between Al and $\delta^{13}C_{carb}$. F. Positive correlation between Al and TOC (one

sample with abnormally high TOC was not considered in this evaluation). G. Weak correlation between Al and $\delta^{13}C_{org}$. (H) Stronger correlation between TOC and $\delta^{13}C_{org}$. Kuancheng section samples (I - L): I. Very weak correlation between Al and $\delta^{13}C_{carb}$. J. Moderate positive correlation between Al and TOC, with R^2=0.33 for TOC >0.05 wt. % carbonates. K. No correlation between Al and $\delta^{13}C_{org}$. L. Two weak correlations between TOC and $\delta^{13}C_{org}$ for low-TOC (<0.05 wt. %) and high-TOC (>0.05 wt. %) carbonates.

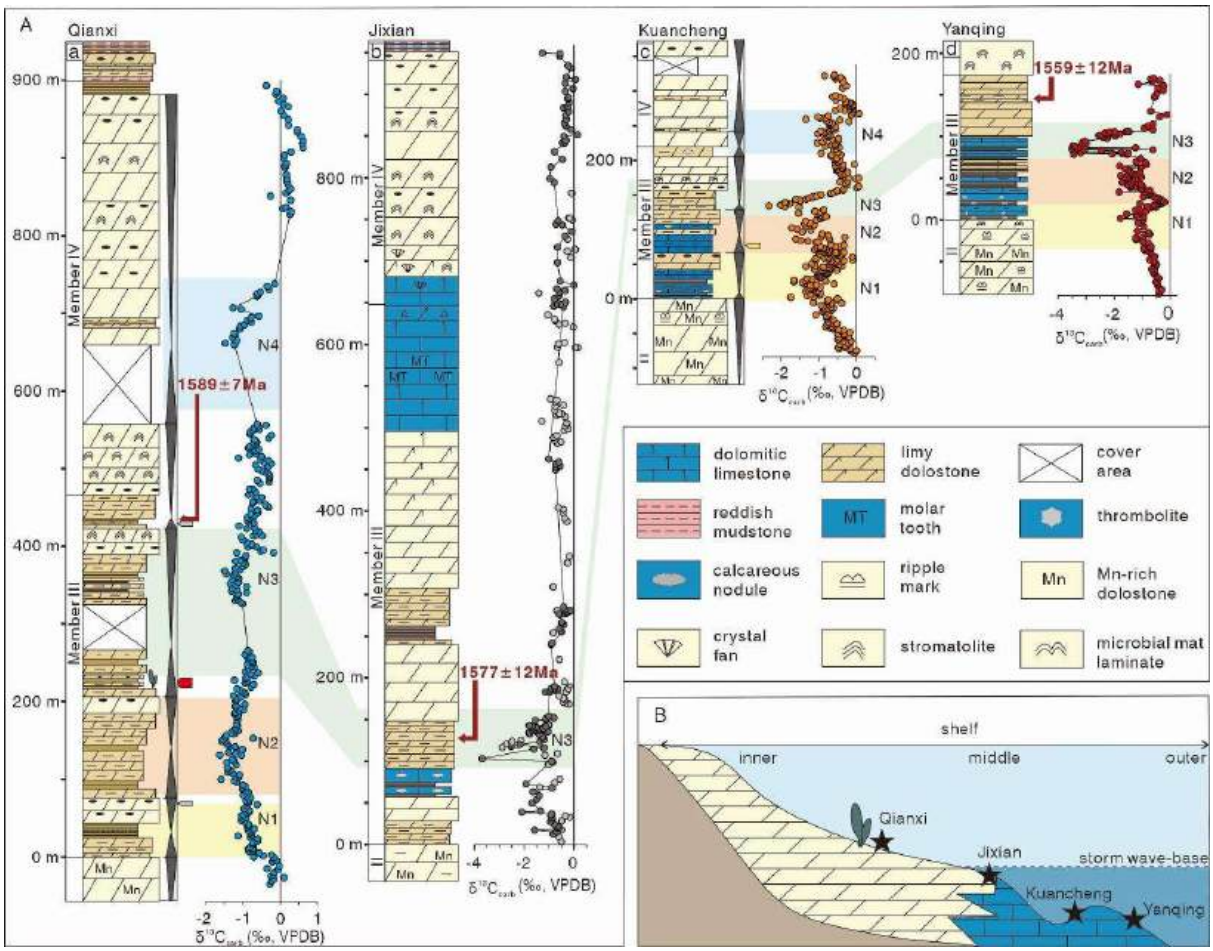

Figure 8. $\delta^{13}C_{carb}$ chemostratigraphy for Gaoyuzhuang members III-IV on the North China Craton. A: Data for Qianxi (a) and Kuancheng (c) were analyzed for this study, while data for the Jixian section (b) are integrated from Zhang et al. (2018) and Luo et al. (2021), and data for the Yanqing section (d) are from Shang et al. (2019). Shading areas denote correlation of the $\delta^{13}C_{carb}$ negative fluctuations and

sedimentary cycles from study sections across different locations. Arrows mark the fossil-hosting horizons (Zhu et al., 2016, Chen et al., 2023). Age constraints source from Li et al., 2010, Tian et al., 2015 and Chen et al., 2024. B: Sedimentary facies of study sections during the deposition of Gaoyuzhuang Member III. See Fig. 1 for lithological key.

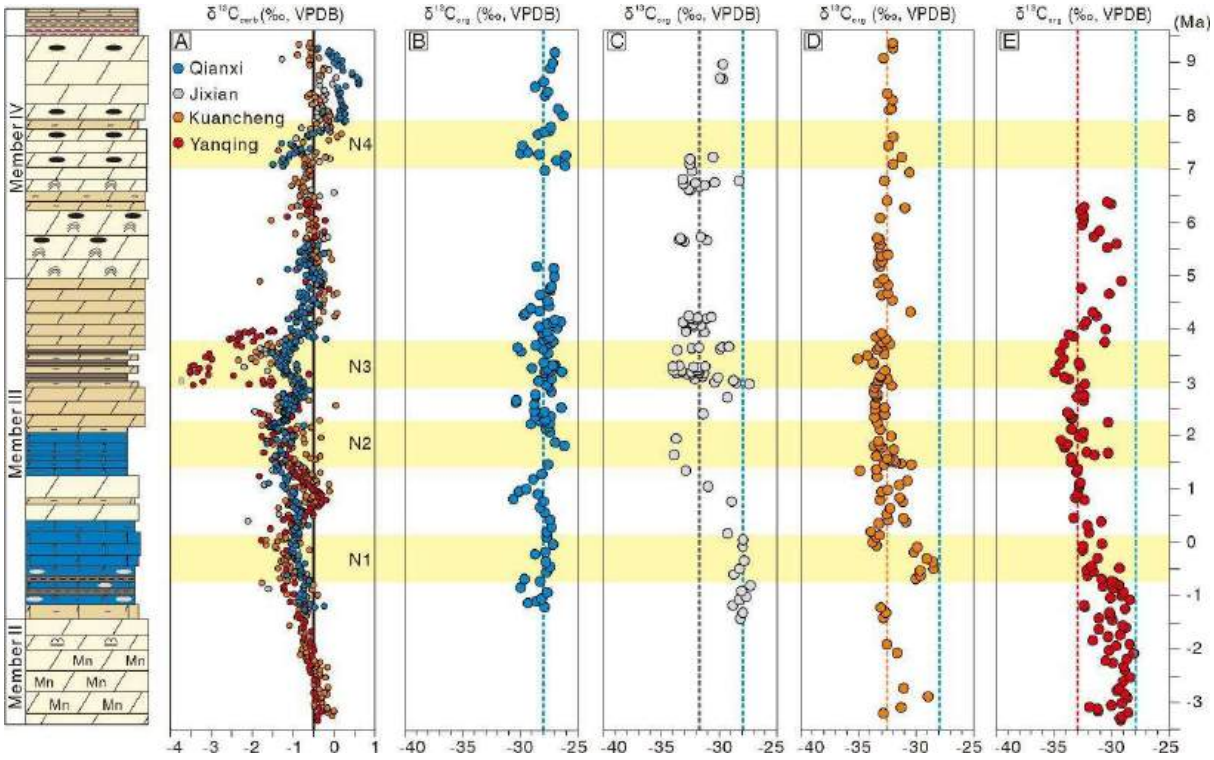

Figure 9. Integrated $\delta^{13}C_{carb}$ curves and $\delta^{13}C_{org}$ data for the four study sections. The astronomical timescale calibration is from Liu et al. (2022). Yellow shading indicates the four $\delta^{13}C_{carb}$ perturbations. Vertical black line indicates the long-term baseline of $\delta^{13}C_{carb}$ composition (A, $\delta^{13}C_{carb}$ = -0.5‰); vertical dashed lines in blue indicate the average $\delta^{13}C_{org}$ value of the Member III of shallow Qianxi section (B, $\delta^{13}C_{org}$ = -28‰) and black, orange and red dash line represent the average $\delta^{13}C_{org}$ value of the Member III of Jixian (C, $\delta^{13}C_{org}$ = -31.75‰), Kuancheng (D, $\delta^{13}C_{org}$ = -32.50‰) and Yanqing (E, $\delta^{13}C_{org}$ = -32.50‰), respectively.

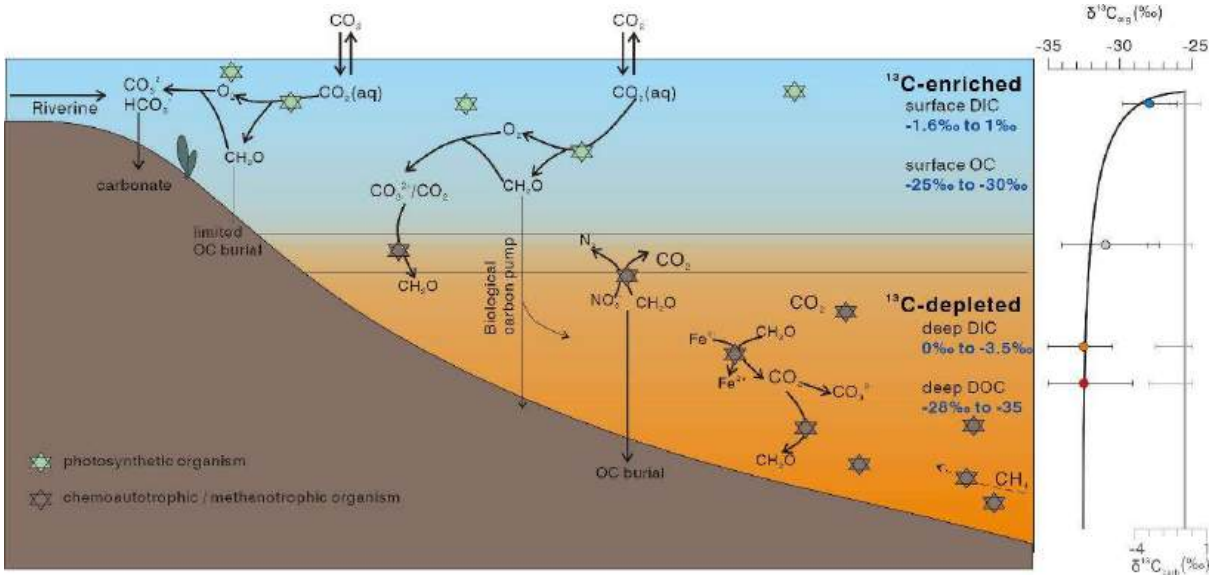

Figure 10. Simplified model of the carbon cycle in the ~1.56 Ga ocean. The large $\delta^{13}C_{org}$ gradient shown on the right was controlled by redox stratification and associated metabolisms, but relatively stable $\delta^{13}C_{carb}$ reflects buffering by a large DIC pool. Blue, grey, orange and red circles denote the average $\delta^{13}C_{org}$ values and variation ranges in Qianxi, Jixian, Kuancheng and Yanqing section, respectively.

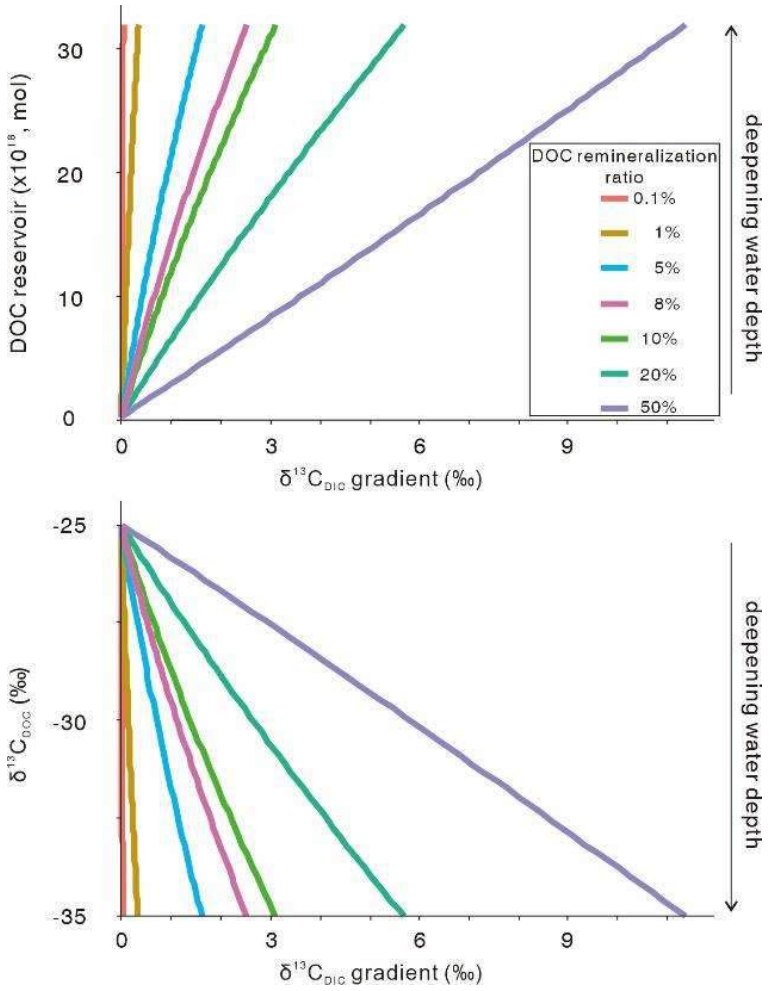

894

895 **Figure 11. Output results of mass balance model calculation.** The results indicate that approximately

896 8% DOC remineralization is required to generate a 2.5‰ $\delta^{13}C_{DIC}$ gradient in the early Mesoproterozoic

897 ocean.